

Back-calculation of the 2017 Piz Cengalo-Bondo landslide cascade with r.avaflow

Martin Mergili, Michel Jaboyedoff, José Pullarelli, Shiva P. Pudasaini

Response to the comments of Referee #1

We would like to thank the reviewer for the constructive remarks. Below, we address each comment in full detail. Our response is written in blue colour. Changes in the manuscript are highlighted in yellow colour.

The authors present an application of the model r.avaflow to the back-calculation of a complex landslide occurred in Switzerland. The case-study is indeed interesting and the scientific question about the two scenario is stimulating (I also really like fig.5). However, as you stated yourself, the investigation of the process through a two-phase numerical model did not allow to discern between the two scenario. So what is really the “take home message” of your work? I do understand that negative results are results but in a way you do not really present them as such. For example, most of your introduction praise the capabilities of two phase depth averaged model in “support the confirmation or rejection of conceptual models” stating the intrinsic epistemological potentiality with respect to one phase models. However, you then proceed with your modelling, that anyhow requires calibration and the selection of vague “physical plausible” parameters, that has numerical issues that constrain you to use “physically implausible” parameters and that do not perform well in the reconstruction of the actual phenomenon. So rather than titling your paper as “back calculation of the 2017: : :” I would suggest to switch it to something such as “challenges and open issues regarding the modelling of the 2017: : :”.

Confirmation and rejection of conceptual models is probably too much emphasized in the introduction of the discussion paper – in fact it is not the main aim of the work to find out which of the two scenarios is the “winner”, but rather to investigate on how well the two scenarios can be reproduced, and what are the main challenges in doing so. The observation of the reviewer that we cannot find out the “winner” scenario while having to optimize the parameters is absolutely correct. We have reformulated the introduction and extended the discussion accordingly (confirmation and rejection of conceptual models are now treated in the discussion). The title, in contrast, is appropriate as it is, we think. The results are far from perfect, of course, but, still, most of the characteristics of the flow can be “reasonably” (see response below) reproduced, and this is only possible with two- or multi-phase models – aspects which are discussed in more detail in the revised manuscript.

These are my other comments regarding your paper

BROAD COMMENTS

1) Optimization and equifinality: The entrainment in your code is calculated with a calibrated coefficient and based on a depth averaged kinetic energy. You defined 6 zones with different friction angles and other calibrated coefficient. How did you suppose it could lead to a selection to confirm or reject a conceptual model (l 51) when, as you stated yourself in the end, there is an obvious problem of equifinality? This issue is common in back analysis, especially when several parameters are involved in

the calibration process. To try to give some “physical plausibility” to the whole parametrization of the backward calculation it is important to:

i) define a straightforward and explicit optimization method

ii) use parameters that are somewhat geotechnically believable with respect to the observed phenomena

iii) provide a clear geomorphological/mechanical reason for each zonation – otherwise of course the more are the zones in which the parameters may be changed, the more the equifinality issue arises.

In my opinion point i) is lacking in your paper. The metrics you use are not so straightforward, especially if you need to jump between two papers to reach their definition and reason of being (is it really Mergili 2018b the best paper to refer to or is it better to go directly to Formetta 2015 and Mergili et al., 2017?). Please devote a paragraph to the interpretation of these metrics rather than cut the discussion off with “indicators of a reasonably good correspondence”. And what is reasonable anyway? Please also show in the picture a zoom of the deposition pattern (modelled and observed) in the alluvial fan. Point ii) is also important. Finding a 45 angle of friction in the E zone is rather “physically un-plausible” as it is, especially when your solid fraction decreases. You discuss this too briefly in the end of the discussion chapter. You have to explain better what is the issue with the code, is the 10 m sampling? is a projection issue related to the conversion of the coordinates? This should be better discussed, also in the light of the new titling of the manuscript. The zoning (point iii) should be more extensively discussed, the definition that it is found in table 1 is too synthetic. For each zone and limit there must be a defined reason to be it that way.

Thank you very much for this detailed and comprehensive comment. It helps us to better formulate some of the main points and challenges of the work:

- Straightforward and explicit (automated) optimization method: in principle, such methods exist in the literature (e.g. Fischer, 2013) and are available to the authors. However, they have been developed for optimizing globally defined parameters (which are constant over the entire study area) against runout length and impact area, and such tools do a very good job for exactly this purpose. However, they cannot directly deal with spatially variable parameters, as they are defined in the present work. With some modifications they might even serve for that – but the main issue is that optimization also considers shapes and maximum values of hydrograph discharges, or travel times at different places of the path. It would be a huge effort to trim optimization algorithms to this purpose, and to make them efficient enough to prevent excessive computational times – we consider this as an important task for the future which is out of scope of the present work. Therefore, we have to use a step-wise expert-based optimization strategy. This is discussed accordingly in the revised manuscript. Regarding the reference parameter set, we still think that Mergili et al. (2018b) is most appropriate, as it is newer than the other papers, therefore based on more experience and a newer version of the software, and closest to the Piz Cengalo-Bondo event in terms of process type (even though much higher in magnitude).

- Plausibility of parameters: the 45° friction angle would only apply if the flow would consist of pure solid. In the simulation, it is reduced linearly with the fluid fraction. As the fluid fraction is commonly >50% in Zone E, the friction angle of the solid is <20°. This aspect, which helps to adapt the effective characteristics of the solid depending on the fluid fraction, is made clear in the revised manuscript. Besides the explanation in the footnote 1) of Table 1, we have added the following sentence at the end of the third paragraph of Section 4 (L226-227): *It is further important to note that δ scales linearly with the solid fraction – this means that the values given in Table 1 only apply for 100% solid.*
- “Reasonably good correspondence”: as there are no fixed criteria available to our knowledge what is a good correspondence, this is to some extent based on expert knowledge, summarizing the essence of Table 3. In Table 3, we have now defined the levels of empirical adequacy: empirically adequate = within the documented range of values; empirically partly adequate = less than 50% away from the documented range of values; empirically inadequate = at least 50% away from the documented range of values. The arithmetic means of minimum and maximum of each range are used for the calculation.
- We have added detail maps of the alluvial fan in Fig. 8 and Fig. 11, showing the observed and simulated impact areas.
- The zones were defined according to geomorphologic criteria and dominant process type. We have tried to formulate this in a clearer way in the revised manuscript. The newly introduced Fig. 4 further illustrates these characteristics and process types, in addition to Table 1.

2) Mass balance: in 220 you write that “only heights <0.25 m are taken into account for the visualization and evaluation of the simulation results”. That’s ok for the visualization part but what about mass balance? how much impact do have diffusion effects in your model? how much material you discard when you filter at 0.25 m?

This is an important point. The threshold of 0.25 m does not affect the mass balance, as it is only applied to visualization and evaluation, but not to the simulation itself. However, there is also a minimum flow height considered in the simulation – a value of 0.01 m was chosen in this case. In scenario 2, the volume of the initial landslide decreased from 3.462 million m³ at release to 3.437 million m³ at deposition, which is 0.7% and therefore negligible, at least for the purpose of the present study. Indeed, loss of material was an issue in the rather channelized Bondasca Valley, where the flow boundary, where loss of material occurs, is large compared to the flow width and flow area: in scenario 1, almost 12% of the flow material “disappeared” due to numerical diffusion until the flow reached the outlet of Val Bondasca. In the revised manuscript, we have reduced the numerical loss of material by recomputing both scenarios, decreasing the minimum flow height for the simulation from 0.01 to 0.001 m: now, the losses until the outlet is reached are below 1% for the Scenario S1, and below 4% for the Scenario S2 for each phase. This has increased the volumes reaching the outlet of Val Bondasca, but did not change the general patterns and messages. Figures and numbers were updated accordingly in the revised manuscript.

SPECIFIC COMMENTS

I 47-49: as a matter of taste I do not think that putting 14 references after a sentence contributes much to the clarity and readability of a paper and to the whole general usefulness for supporting a scientific discourse (that should be the main reason for inserting citations in an introduction)

The intention of the large number of references put here was to highlight the importance of the topic and to strongly support the statements. However, we can follow the argument of the reviewer and have reduced the number of references to four articles published in the last ten years.

I 88: insert a couple of words to explain how these displacements were monitored

This information was added: mainly radar interferometry, but also laser scanning was applied to measure the displacements.

I 94 and following: check that each acronym has its own definition the first time they appear in the text. Moreover the VAW and WSL reports are written in German so it is not easy to extract the required information. Please if you refer to these works add a sentence summarizing the useful findings.

We have added an introductory paragraph to Section 2.2, where the abbreviations are explained (L89-92):

“The complex landslide which occurred on 23 August 2017 was documented mainly by reports of the Swiss Federal Institute for Forest, Snow and Landscape Research (WSL), the Laboratory of Hydraulics, Hydrology and Glaciology (VAW) of the ETH Zurich, and the Amt für Wald und Naturgefahren (Office for Forest and Natural Hazards) of the canton of Grisons.”

Those main points of these sources which are relevant for the present work are mentioned in the text, particularly in the sections 2.2 and 2.3.

I 100-102: insert data about the average steepness of the tract. In fact in the whole paper little information about the local heights and steepness are inferable. In Fig 1 the contour lines labels are missing and in the following maps the contour lines are missing altogether. I would suggest the authors to add the labels in fig. 1 and to insert a table or a figure with the average steepness of the channel profile in each of the 6 zones.

Indeed, this is an important point. In the revised manuscript we provide an additional figure (the new Fig. 4) showing a profile of the path with the elevation and slope information added, and also some information with regard to the individual zones. For this purpose, we have re-analyzed the geometric properties and included some minor updates of travel distances, drop heights, and angles of reach. Further, Fig. 1 has been equipped with contour line labels.

I 109: is it possible to talk about rock avalanche with an angle of reach of 28 and no brandung? refer to Nicoletti 1991, Corominas 1996 and Hungr 2005 and discuss

We follow the revised Varnes classification (Hungr et al., 2014) – there, rock avalanches are essentially described as pieces of rock moving as one mass like a flow, instead of individual blocks. This clearly corresponds to those descriptions of the event in Zone C which are available to us. Nevertheless, we fully

agree that the issue of the angle of reach and run-up is very relevant in this context, deserving some further attention. Therefore, we have added the following text (L111-115):

“This value is lower than the 22° predicted by the equation of Scheidegger (1973), probably due to the sharp deflection of the initial landslide. Following the concept of Nicoletti and Sorriso-Valvo (1991), the rock avalanche was characterized by channelling of the mass. Only a limited run-up was observed, probably due to the gentle horizontal curvature of the valley in that area (no orthogonal impact on the valley slope; Hewitt, 2002).”

Corominas (1996) and Hungr et al. (2005) do not explicitly consider rock avalanches, but other types of landslides, so in our opinion it would not be appropriate to include these references here.

I 116: did you filter the errors in the volume estimation? If yes, how?

The volume was calculated comparing the DSM made by photogrammetry and the DEM from the government with a 2 m resolution. Errors might come from the fact that we compare the 2017 DSM with a DEM previous to the 2011 event. The structures on the surface were used to exclude the 2011 volume, a procedure connected to an uncertainty of few 100,000s of cubic metres, when comparing the most plausible boundaries between the release areas of the two events. This may also explain the slight discrepancies between the volumes reported in different sources. Compared to the initial manuscript, we have revised the volume estimate and arrived at 3.2–3.3 million m³ for the initial rock slide, which corresponds better to other reports than the initial estimate of almost 3.5 million m³ (see the updated Fig. 5). No further filtering was carried out.

Fig 8 – please put hydrograph a and b to the left

We have rearranged the panes of Fig. 8 accordingly.

Back-calculation of the 2017 Piz Cengalo-Bondo landslide cascade with r.avaflow

Martin Mergili^{1,2}, Michel Jaboyedoff³, José Pullarello³, Shiva P. Pudasaini⁴

¹ Institute of Applied Geology, University of Natural Resources and Life Sciences (BOKU), Peter-Jordan-Straße 82, 1190 Vienna, Austria

² Geomorphological Systems and Risk Research, Department of Geography and Regional Research, University of Vienna, Universitätsstraße 7, 1010 Vienna, Austria

³Institute of Earth Sciences, University of Lausanne, Quartier UNIL-Mouline, Bâtiment Géopolis, 1015 Lausanne, Switzerland

⁴ Institute of Geosciences, Geophysics Section, University of Bonn, Meckenheimer Allee 176, 53115 Bonn, Germany

Correspondence to: M. Mergili (martin.mergili@boku.ac.at)

Abstract

In the morning of 23 August 2017, around 3 million m³ of granitoid rock broke off from the east face of Piz Cengalo, SE Switzerland. The initial rock slide-rock fall entrained 0.6 million m³ of a glacier and continued as a rock(-ice) avalanche, before evolving into a channelized debris flow that reached the village of Bondo at a distance of 6.5 km after a couple of minutes. Subsequent debris flow surges followed in the next hours and days. The event resulted in eight fatalities along its path and severely damaged Bondo. The most likely candidates for the water causing the transformation of the rock avalanche into a long-runout debris flow are the entrained glacier ice and water originating from the debris beneath the rock avalanche. In the present work we try to reconstruct conceptually and numerically the cascade from the initial rock slide-rock fall to the first debris flow surge and thereby consider two scenarios in terms of qualitative conceptual process models: (i) entrainment of most of the glacier ice by the frontal part of the initial rock slide-rock fall and/or injection of water from the basal sediments due to sudden rise in pore pressure, leading to a frontal debris flow, with the rear part largely remaining dry and depositing mid-valley; and (ii) most of the entrained glacier ice remaining beneath/behind the frontal rock avalanche, and developing into an avalanching flow of ice and water, part of which overtops and partially entrains the rock avalanche deposit, resulting in a debris flow. Both scenarios can be numerically reproduced with the two-phase mass flow model (Pudasaini, 2012) implemented with the simulation software r.avaflow, based on plausible assumptions of the model parameters. However, these simulation results do not allow to conclude on which of the two scenarios is the more likely one. Future work will be directed towards the application of a three-phase flow model (rock, ice, fluid) including phase transitions, in order to better represent the melting of glacier ice, and a more appropriate consideration of deposition of debris flow material along the channel.

Keywords: Debris flow, Entrainment, High-mountain process chain, Rock avalanche, Two-phase flow model, r.avaflow

1 Introduction

Landslides lead to substantial damages to life, property, and infrastructures every year. Whereas initial landslides in hilly terrain have mostly local effects, landslides in high-mountain areas, with elevation differences of thousands of metres over a few kilometres may form the initial points of process chains which, due to their interactions with glacier ice, snow, lakes, or basal material, sometimes evolve into long-runout debris avalanches, debris flows or floods. Such complex landslide events may occur in remote areas, such as the 2012 Alpl rock-snow avalanche in Austria (Preh and Sausgruber, 2015) or the 2012 Santa Cruz multi-lake outburst event in Peru (Mergili et al., 2018a). If they reach inhabited areas, such events lead to major destruction even several kilometres away from the source and have led to major disasters in the past, such as the 1949 Khait rock avalanche-loess flow in Tajikistan (Evans et al., 2009b); the 1962 and 1970 Huascarán rock fall-debris avalanche events in Peru (Evans et al., 2009a; Mergili et al., 2018b); the 2002 Kolka-Karmadon ice-rock avalanche in Russia (Huggel et al., 2005); the 2012 Seti River debris flood in Nepal (Bhandari et al., 2012); or the 2017 Piz Cengalo-Bondo rock avalanche-debris flow event in Switzerland. The initial fall or slide sequences of such process chains are commonly related to a changing cryosphere such as glacial debuttressing, the formation of hanging glaciers, or a changing permafrost regime (Harris et al., 2009; Krautblatter et al., 2013; Haeberli and Whiteman, 2014; Haeberli et al., 2017).

Computer models assist risk managers in anticipating the impact areas, energies, and travel times of complex mass flows. Conventional single-phase flow models, considering a mixture of solid and fluid components (e.g. Voellmy, 1955; Savage and Hutter, 1989; Iverson, 1997; McDougall and Hungr, 2004; Christen et al., 2010), do not serve for such a purpose. Instead, simulations rely on (i) model cascades, changing from one approach to the next at each process boundary (Schneider et al., 2014; Somos-Valenzuela et al., 2016); or (ii) bulk mixture models or two- or even multi-phase flow models (Pitman and Le, 2005; Pudasaini, 2012; Iverson and George, 2014; Mergili et al., 2017). Worni et al. (2014) have highlighted the advantages of (ii) for considering also the process interactions and boundaries. Two- or multi-phase flow models separately consider the solid and the fluid phase, but also phase interactions.

The aim of the present work is to learn about our ability to reproduce sophisticated transformation mechanisms involved in complex, cascading landslide processes, with GIS-based tools. For this purpose, we apply the computational tool r.avaflow (Mergili et al., 2017), which employs an enhanced version of the Pudasaini (2012) two-phase flow model, to back-calculate the 2017 Piz Cengalo-Bondo landslide cascade in SE Switzerland, which was characterized by the transformation of a rock avalanche to a long-runout debris flow. We consider two scenarios in terms of hypothetical qualitative conceptual models of the physical transformation mechanisms. On this basis, we try to numerically reproduce these scenarios, satisfying the requirements of physical plausibility of the model parameters, and empirical adequacy in terms of correspondence of the results with the documented and inferred impact areas, volumes, velocities, and travel times. Based on the outcomes, we identify the key challenges to be addressed in future research.

Thereby we rely on the detailed description, documentation, and topographic reconstruction of this recent event. The event documentation, data used, and the conceptual models are outlined in Section 2. We briefly introduce the simu-

68 lation framework r.avaflow (Section 3) and explain its parametrization and our simulation strategy (Section 4) before
69 presenting (Section 5) and discussing (Section 6) the results obtained. Finally, we conclude with the key messages of
70 the study (Section 7).

71 **2 The 2017 Piz Cengalo-Bondo landslide cascade**

72 **2.1 Piz Cengalo and Val Bondasca**

73 The Val Bondasca is a left tributary valley to the Val Bregaglia in the canton of the Grisons in SE Switzerland (Fig. 1).
74 The Bondasca stream joins the Mera River at the village of Bondo at 823 m asl. It drains part of the Bregaglia Range,
75 built up by a mainly granitic intrusive body culminating at 3678 m asl. Piz Cengalo, with a summit elevation of
76 3368 m asl, is characterized by a steep, intensely fractured NE face which has repeatedly been the scene of landslides,
77 and which is geomorphologically connected to the Val Bondasca through a steep glacier forefield. The glacier itself has
78 largely retreated to the cirque beneath the rock wall.

79 On 27 December 2011, a rock avalanche with a volume of 1.5–2 million m³ developed out of a rock toppling from the
80 NE face of Piz Cengalo, travelling for a distance of 1.5 km down to the uppermost part of the Val Bondasca (Haeber-
81 li et al., 2013; De Blasio and Crosta, 2016; Amann et al., 2018). This rock avalanche reached the main torrent channel.
82 Erosion of the deposit thereafter resulted in increased debris flow activity (Frank et al., 2019). No entrainment of glaci-
83 er ice was documented for this event. As blue ice had been observed directly at the scarp, the role of permafrost for
84 the rock instability was discussed. An early warning system was installed and later extended (Steinacher et al., 2018).
85 Displacements at the scarp area, measured by radar interferometry and laser scanning, were few centimetres per year
86 between 2012 and 2015, and accelerated in the following years. In early August 2017, increased rock fall activity and
87 deformation rates alerted the authorities. A major rock fall event occurred on 21 August 2017 (Amann et al., 2018).

88 **2.2 The event of 23 August 2017**

89 The complex landslide which occurred on 23 August 2017 was documented mainly by reports of the Swiss Federal
90 Institute for Forest, Snow and Landscape Research (WSL), the Laboratory of Hydraulics, Hydrology and Glaciology
91 (VAW) of the ETH Zurich, and the Amt für Wald und Naturgefahren (Office for Forest and Natural Hazards) of the
92 canton of Grisons.

93 At 9:31 am local time, a volume of approx. 3 million m³ detached from the NE face of Piz Cengalo, as indicated by
94 WSL (2017); Amann et al. (2018); and the point cloud we obtained through structure from motion using pictures tak-
95 en after the event. Documented by videos and by seismic records (Walter et al., 2018), it impacted the glacier beneath
96 the rock face and entrained approx. 0.6 million m³ of ice (VAW, 2017; WSL, 2017), was sharply deflected at an oppo-
97 site rock wall, and evolved into a rock(-ice) avalanche. Part of this avalanche immediately converted into a debris flow
98 which flowed down the Val Bondasca. It was detected at 9:34 by the debris flow warning system which had been in-
99 stalled near the hamlet of Prä approx. 1 km upstream from Bondo. According to different sources, the debris flow

100 surge arrived at Bondo between 9:42 (derived from WSL, 2017) and 9:48 (Amt für Wald und Naturgefahren, 2017).
101 The rather low velocity in the lower portion of the Val Bondasca is most likely a consequence of the narrow gorge
102 topography, and of the viscous behaviour of this first surge. Whereas approx. 540,000 m³ of material were involved,
103 only 50,000 m³ arrived at Bondo immediately (data from the Canton of Grisons reported by WSL, 2017). The remain-
104 ing material was partly remobilized by six further debris flow surges recorded during the same day, one on 25 August,
105 and one – triggered by rainfall – on 31 August 2017. All nine surges together deposited a volume of approx. 500,000–
106 800,000 m³ in the area of Bondo, less than half of which was captured by a retention basin (Bonanomi and Keiser,
107 2017).

108 The vertical profile of the main flow path is illustrated in Fig. 4. The total angle of reach of the process chain from the
109 initial release down to the outlet of the Bondasca Valley was approx. 17.4°, computed from the travel distance of
110 7.0 km and the vertical drop of approx. 2.2 km. The initial landslide to the terminus of the rock avalanche showed an
111 angle of reach of approx. 25.8°, derived from the travel distance of 3.4 km and the vertical drop of 1.7 km. This value is
112 lower than the 22° predicted by the equation of Scheidegger (1973), probably due to the sharp deflection of the initial
113 landslide. Following the concept of Nicoletti and Sorriso-Valvo (1991), the rock avalanche was characterized by chan-
114 nelling of the mass. Only a limited run-up was observed, probably due to the gentle horizontal curvature of the valley
115 in that area (no orthogonal impact on the valley slope; Hewitt, 2002). There were eight fatalities, concerning hikers in
116 the Val Bondasca, extensive damages to buildings and infrastructures, and evacuations for several weeks or even
117 months.

118 2.3 Data and conceptual model

119 Reconstruction of the rock and glacier volumes involved in the event was based on an overlay of a 2011 swisstopo
120 MNS-Digital Elevation Model (DEM) (contract: swisstopo–DV084371), derived through airborne laser scanning in
121 2011 and available at a raster cell size of 2 m, and a Digital Surface Model (DSM) obtained through Structure from
122 Motion (SfM) techniques after the 2017 event. This analysis resulted in a detached rock volume of 3.27 million m³,
123 which is slightly more than the value of 3.15 million m³ reported by Amann et al. (2018), and an entrained ice volume
124 of 770,000 m³ (Fig. 5). However, these volumes neglect smaller rock falls before and after the large 2017 event, and
125 also glacial retreat. The 2011 event took place after the DTM had been acquired, but it released from an area above the
126 2017 scarp. The boundary between the 2011 and the 2017 scarps, however, is slightly uncertain, which explains the
127 discrepancies between the different volume reconstructions. Assuming some minor entrainment of the glacier ice in
128 2011 and some glacial retreat, we arrive at an entrained ice volume of 600,000 m³, a value which is very well support-
129 ed by VAW (2017).

130 There is still disagreement on the origin of the water having led to the debris flow, particularly to the first surge. Bo-
131 nanomi and Keiser (2017) clearly mention meltwater from the entrained glacier ice as the main source, whereby much
132 of the melting is assigned to impact, shearing and frictional heating directly at or after impact, as it is often the situa-
133 tion in rock-ice avalanches (Pudasaini and Krautblatter, 2014). WSL (2017) has shown, however, that the energy re-

134 leased was only sufficient to melt approx. half of the glacier ice. Water pockets in the glacier or a stationary water
135 source along the path might have played an important role (Demmel, 2019). Walter et al. (2019) claim that much of
136 the glacier ice was crushed, ejected and dispersed (Fig. 3b), whereas water injected into the rock avalanche due to pore
137 pressure rise in the basal sediments would have played a major role. In any case, the development of a debris flow
138 from a landslide mass with an overall solid fraction of as high as ~ 0.85 (considering the water equivalent of the glacier
139 ice) requires some spatio-temporal differentiation of the water/ice content. We consider two qualitative conceptual
140 models – or scenarios – possibly explaining such a differentiation:

141 S1 The initial rock slide-rock fall led to massive entrainment, fragmenting and melting of glacier ice, mixing of
142 rock with some of the entrained ice and the meltwater, and injection of water from the basal sediments into
143 the rock avalanche mass quickly upon impact due to overload-induced pore pressure rise. As a consequence,
144 the front of the rock avalanche was characterized by a high content of ice and water, highly mobile, and
145 therefore escaped as the first debris flow surge, whereas the less mobile rock avalanche behind – still with
146 some water and ice in it – decelerated and deposited mid-valley. The secondary debris flow surges occurred
147 mainly due to backwater effects. This scenario largely follows the explanation of Walter et al. (2019) that the
148 first debris flow surge was triggered at the front of the rock avalanche by overload and pore pressure rise,
149 whereas the later surges overtopped the rock avalanche deposits, as indicated by the surficial scour patterns.

150 S2 The initial rock slide-rock fall impacted and entrained the glacier. Most of the entrained ice remained beneath
151 and developed into an avalanching flow of melting ice behind the rock avalanche. The rock avalanche decel-
152 erated and stopped mid-valley. Part of the avalanching flow overtopped and partly entrained the rock ava-
153 lanche deposit – leaving behind the scour traces observed in the field – and evolved into the channelized de-
154bris flow which arrived at Bondo a couple of minutes later. The secondary debris flow surges started from the
155 rock avalanche deposit due to melting and infiltration of the remaining ice, and due to backwater effects. This
156 scenario is similar to the theory developed at the WSL Institute for Snow and Avalanche Research (SLF), who
157 also did a first simulation of the rock avalanche (WSL, 2017).

158 Fig. 6 illustrates the conceptual models attempting to explain the key mechanisms involved in the rock avalanche-
159 debris flow transformation.

160 3 The simulation framework r.avaflow

161 r.avaflow represents a comprehensive GIS-based open source framework which can be applied for the simulation of
162 various types of geomorphic mass flows. In contrast to most other mass flow simulation tools, r.avaflow utilizes a gen-
163 eral two-phase-flow model describing the dynamics of the mixture of solid particles and viscous fluid and the strong
164 interactions between these phases. It further considers erosion and entrainment of surface material along the flow
165 path. These features facilitate the simulation of cascading landslide processes such as the 2017 Piz Cengalo-Bondo
166 event. r.avaflow is outlined in full detail by Mergili and Pudasaini (2019). The code, a user manual, and a collection of

167 test datasets are available from Mergili (2019). Only those aspects directly relevant for the present work are described
168 in this section.

169 Essentially, the Pudasaini (2012) two-phase flow model is employed for computing the dynamics of mass flows moving
170 from a defined release area (solid and/or fluid heights are assigned to each raster cell) or release hydrograph (at each
171 time step, solid and/or fluid heights are added at a given profile, moving at a given cross-profile velocity) down
172 through a DEM. The spatio-temporal evolution of the flow is approximated through depth-averaged solid and fluid
173 mass and momentum balance equations (Pudasaini, 2012). This system of equations is solved through the TVD-NOC
174 Scheme introduced by Nussyahu and Tadmor (1990), adapting an approach presented by Tai et al. (2002) and Wang et
175 al. (2004). The characteristics of the simulated flow are governed by a set of flow parameters (some of them are shown
176 in the Tables 1 and 2). Compared to the Pudasaini (2012) model, some extensions have been introduced which include
177 (i) ambient drag or air resistance (Kattel et al., 2016; Mergili et al., 2017); and (ii) fluid friction, governing the influ-
178 ence of basal surface roughness on the fluid momentum (Mergili et al., 2018b). Both extensions rely on empirical coef-
179 ficients, C_{AD} for the ambient drag and C_{FF} for the fluid friction. Further, drag and viscosity are computed according to
180 enhanced concepts. As in Domnik et al. (2013) and Pudasaini and Mergili (2019), the fluid viscosity is enhanced by the
181 yield strength. Most importantly, the internal friction angle φ and the basal friction angle δ of the solid are scaled with
182 the solid fraction in order to approximate effects of reduced interaction between the solid particles and the basal sur-
183 face in fluid-rich flows.

184 Entrainment is calculated through an empirical model. In contrast to Mergili et al. (2017), where an empirical en-
185 trainment coefficient is multiplied with the momentum of the flow, here we multiply the entrainment coefficient
186 C_E ($s\ kg^{-1}\ m^{-1}$) with the kinetic energy of the flow:

$$187 \quad q_{E,s} = C_E |T_s + T_f| \alpha_{s,E}, \quad q_{E,f} = C_E |T_s + T_f| (1 - \alpha_{s,E}), \quad (1)$$

188 where $q_{E,s}$ and $q_{E,f}$ ($m\ s^{-1}$) are the solid and fluid entrainment rates, T_s and T_f (J) are the kinetic energies of the solid and
189 fluid fractions of the flow, and $\alpha_{s,E}$ is the solid fraction of the entrainable material. Solid and fluid flow heights and
190 momenta, and the change of the basal topography, are updated at each time step (see Mergili et al., 2017 for details).

191 As r.avaflow operates on the basis of GIS raster cells, its output essentially consists of raster maps –for all time steps
192 and for the overall maximum – of solid and fluid flow heights, velocities, pressures, kinetic energies, and entrained
193 heights. In addition, output hydrograph profiles may be defined at which solid and fluid heights, velocities, and dis-
194 charges are provided at each time step.

195 **4 Parameterization of r.avaflow**

196 One set of simulations is performed for each of the Scenarios S1 and S2 (Fig. 6), considering the process chain from the
197 release of the rock slide-rock fall to the arrival of the first debris flow surge at Bondo. Neither triggering of the event
198 nor subsequent surges or distal debris floods beyond Bondo are considered in this study. Equally, the dust cloud associ-

199 ated to the rock avalanche (WSL, 2017) is not the subject here. Initial sliding of the glacier beneath the rock ava-
200 lanche, as assumed in **Scenario S2**, cannot directly be modelled. That would require a three-phase model, which is
201 beyond the scope here. Instead, release of the glacier ice and meltwater is assumed in a separate simulation after the
202 rock avalanche has passed over it. We consider this workaround an acceptable approximation of the postulated scenar-
203 io (Section 6).

204 We use the 2011 swisstopo MNS-DEM, corrected for the rock slide-rock fall scarp and the entrained glacier ice by
205 overlay with the 2017 SfM DSM (Section 2). The maps of release height and maximum entrainable height are derived
206 from the difference between the 2011 swisstopo DTM and the 2017 SfM DSM (**Fig. 5**; Section 2). The release mass is
207 considered completely solid, whereas the entrained glacier is assumed to contain some solid fraction (coarse till). The
208 glacier ice is assumed to melt immediately on impact and is included in the fluid along with fine till. We note that the
209 fluid phase does not represent pure water, but a mixture of water and fine particles (Table 2). The fraction of the glaci-
210 er allowed to be incorporated in the process chain is empirically optimized (Table 3). Based on the same principle, the
211 maximum depth of entrainment of fluid due to pore pressure overload in **Scenario S1** is set to 25 cm, whereas the max-
212 imum depth of entrainment of the rock avalanche deposit in **Scenario S2** is set to 1 m.

213 The study area is divided into six zones A–F (**Fig. 4 and Fig. 7**; Table 1). Each of these zones represents an area with
214 particular **geomorphic characteristics and dominant process types**, which can be translated into model parameters.
215 Due to the impossibility to directly measure the key parameters in the field (Mergili et al., 2018a, b), the parameters
216 summarized in Table 1 and Table 2 are the result of an iterative optimization procedure, where multiple simulations
217 with different parameter sets are performed in order to arrive at one “optimum” simulation for each scenario. It is
218 thereby important to note that we largely derive one single set of optimized parameters, which is valid for both of the
219 scenarios. Optimization criteria are (i) the empirical adequacy of the model results, and (ii) the physical plausibility of
220 the parameters. Thereby, the empirical adequacy is quantified through comparison of the results with the documented
221 impact area, the travel times to the output hydrograph profiles O2, O3, and O4 (**Fig. 7**), and the reported volumes
222 (Amt für Wald und Naturgefahren, 2017; Bonanomi and Keiser, 2017; WSL, 2017). The physical plausibility of the
223 model parameters is evaluated on the basis on the parameters suggested by Mergili et al. (2017) and on the findings of
224 Mergili et al. (2018a, b). The values of the basal friction angle (δ), the ambient drag coefficient (C_{AD}), the fluid friction
225 coefficient (C_{FF}), and the entrainment coefficient (C_E) are differentiated between and within the zones (Table 1),
226 whereas global values are defined for all the other parameters (Table 2). **It is further important to note that δ scales
227 linearly with the solid fraction – this means that the values given in Table 1 only apply for 100% solid.**

228 Durations of $t = 1800$ s are considered for both scenarios. At this point of time, the first debris flow surge has largely
229 passed and left the area of interest, except for some remaining tail of fluid material. Only heights ≥ 0.25 m are taken
230 into account for the visualization and evaluation of the simulation results. Considering the size of the event, a cell size
231 of 10 m is considered the best compromise between capturing a sufficient level of detail and ensuring an adequate
232 computational efficiency, and is therefore applied for all simulations.

234 **5.1 Scenario S1 – Frontal debris flow surge**

235 Fig. 8 illustrates the distribution of the simulated maximum flow heights, maximum entrained heights, and deposition
 236 area after $t = 1800$ s, when most of the initial debris flow surge has passed the confluence of the Bondasca stream and
 237 the Maira river. The comparison of observed and simulated impact areas results in a critical success index $CSI = 0.558$,
 238 a distance to perfect classification $D2PC = 0.167$, and a factor of conservativeness $FoC = 1.455$. These performance in-
 239 dicators are derived from the confusion matrix of true positives, true negatives, false positives, and false negatives. CSI
 240 and $D2PC$ measure the correspondence of the observed and simulated impact areas. Both indicators can range between
 241 0 and 1, whereby values of CSI close to 1 and values of $D2PC$ close to 0 point to a good correspondence. FoC indicates
 242 whether the observed impact areas are overestimated ($FoC > 1$), or underestimated by the simulation ($FoC < 1$). More
 243 details are provided by Formetta et al. (2015) and by Mergili et al. (2017, 2018a).

244 Interpreting these values as indicators for a reasonably good correspondence between simulation and observation in
 245 terms of impact area, we now consider the dimension of time, focussing on the output hydrographs OH1–OH4 (Fig. 9;
 246 see Fig. 7 and Fig. 8 for the location of the corresponding hydrograph profiles O1–O4). Much of the rock avalanche
 247 passes the profile O1 between $t = 60$ s and $t = 100$ s. OH2 (Fig. 9a; located in the upper portion of Val Bondasca) sets on
 248 before $t = 140$ s and quickly reaches its peak, with a volumetric solid ratio of approx. 30% (maximum $900 \text{ m}^3/\text{s}$ of solid
 249 and $2,200 \text{ m}^3/\text{s}$ of fluid discharge). Thereafter, this first surge quickly tails off. The solid flow height, however, increas-
 250 es to around 3 m and remains so until the end of the simulation, whereas the fluid flow height slowly and steadily tails
 251 off. Until $t = 1800$ s the profile O2 is passed by a total of $221,000 \text{ m}^3$ of solid and $308,000 \text{ m}^3$ of fluid material (the fluid
 252 representing a mixture of fine mud and water with a density of $1,400 \text{ kg m}^{-3}$; see Table 2). The hydrograph profile O3
 253 in Prä, approx. 1 km upstream of Bondo, is characterized by a surge starting before $t = 280$ s and slowly tailing off af-
 254 terwards. Discharge at the hydrograph OH4 (Fig. 9b; O4 is located at the outlet of the canyon to the debris fan of
 255 Bondo) starts at around $t = 700$ s and reaches its peak of solid discharge at $t = 1020$ s ($167 \text{ m}^3/\text{s}$). Solid discharge de-
 256 creases thereafter, whereas the flow becomes fluid-dominated with a fluid peak of $202 \text{ m}^3/\text{s}$ at $t = 1320$ s. The maxi-
 257 mum total flow height simulated at O4 is 2.53 m. This site is passed by a total of $91,000 \text{ m}^3$ of solid and $175,000 \text{ m}^3$ of
 258 fluid material, according to the simulation – an overestimate, compared to the documentation (Table 3).

259 Fig. 10 illustrates the travel time and the frontal velocities of the rock avalanche and the initial debris flow. The initial
 260 surge reaches the hydrograph profile O3 – located 1 km upstream of Bondo – at $t = 280$ s (Fig. 10a; Fig. 9c). This is in
 261 line with the documented arrival of the surge at the nearby monitoring station (Table 3). Also the simulated travel
 262 time to the profile O4 corresponds to the – though uncertain – documentation. The initial rock avalanche is character-
 263 ized by frontal velocities $>25 \text{ m/s}$, whereas the debris flow largely moves at $10\text{--}25 \text{ m/s}$. Velocities drop below 5 m/s
 264 in the lower part of the valley (Zone E) (Fig. 10b).

5.2 Scenario S2 – Debris flow surge by overtopping and entrainment of rock avalanche

Fig. 11 illustrates the distribution of the simulated maximum flow heights, maximum entrained heights, and deposition area after $t = t_0 + 1740$ s, where t_0 is the time between the release of the initial rock avalanche and the mobilization of the entrained glacier. The simulated impact and deposition areas of the initial rock avalanche are also shown in Fig. 11. However, we now concentrate to the debris flow, triggered by the entrainment of $145,000 \text{ m}^3$ of solid material from the rock avalanche deposit. Flow heights – as well as the hydrographs presented in Fig. 9c and d and the temporal patterns illustrated in Fig. 12 – only refer to the debris flow developing from the entrained glacier and the entrained rock avalanche material. The confusion matrix of observed and simulated impact areas reveals partly different patterns of performance than for the Scenario S1: $CSI = 0.590$; $D2PC = 0.289$; and $FoC = 0.925$. The lower FoC value and the lower performance in terms of $D2PC$ reflect the missing initial rock avalanche in the simulation results. The output hydrographs OH2 and OH4 differ from the hydrographs obtained through the Scenario S1, but also show some similarities (Fig. 9c and d). Most of the flow passes through the hydrograph profile O1 between $t = t_0 + 40$ s and $t_0 + 80$ s, and through O2 between $t = t_0 + 100$ s and $t_0 + 180$ s. The hydrograph OH2 is characterized by a short peak of $3,500 \text{ m}^3/\text{s}$ of solid and $4,500 \text{ m}^3/\text{s}$ of fluid, with a volumetric solid fraction of 0.44 and quickly decreasing discharge afterwards (Fig. 9c). In contrast to Scenario S1, flow heights drop steadily, with values below 2 m from $t = t_0 + 620$ s onwards. The hydrograph OH3 is characterized by a surge starting around $t = t_0 + 240$ s. Discharge at the hydrograph OH4 (Fig. 9d) sets on around $t = t_0 + 600$ s, and the solid peak of $240 \text{ m}^3/\text{s}$ is simulated at approx. $t = t_0 + 780$ s. The delay of the peak of fluid discharge is more pronounced when compared to Scenario S1 ($310 \text{ m}^3/\text{s}$ at $t = t_0 + 960$ s). Profile O4 is passed by a total of $65,000 \text{ m}^3$ of solid and $204,000 \text{ m}^3$ of fluid material. The volumetric solid fraction drops from above 0.60 at the very onset of the hydrograph to around 0.10 (almost pure fluid) at the end. The maximum total flow height at O4 is 3.1 m.

Fig. 12 illustrates the travel times and the frontal velocities of the rock avalanche and the initial debris flow. Assuming that t_0 is in the range of some tens of seconds, the time of arrival of the surge at O3 is in line with the documentation also for the Scenario S2 (Fig. 12a; Table 3). The frontal velocity patterns along Val Bondasca are roughly in line with those derived in the Scenario S1 (Fig. 12b). However, the scenarios differ among themselves in terms of the more pronounced, but shorter peaks of the hydrographs in Scenario S2 (Fig. 9). This pattern is a consequence of the more sharply defined debris flow surge. In Scenario S1, the front of the rock avalanche deposit constantly “leaks” into Val Bondasca, providing supply for the debris flow also at later stages. In Scenario S2, entrainment of the rock avalanche deposit occurs relatively quickly, without material supply afterwards. This type of behaviour is strongly coupled to the value of C_E and the allowed height of entrainment chosen for the rock avalanche deposit.

6 Discussion

Our simulation results reveal a reasonable degree of empirical adequacy and physical plausibility with regard to most of the reference observations. Having said that, we have also identified some important limitations which are now

298 discussed in more detail. First of all, we are not able to decide on the more realistic of the two **Scenarios S1 and S2**. In
299 general, the melting and mobilization of glacier ice upon rock slide-rock fall impact is hard to quantify from straight-
300 forward calculations of energy transformation, as Huggel et al. (2005) have demonstrated on the example of the 2002
301 Kolka-Karmadon event. In the present work, the assumed amount of melting (approx. half of the glacier ice) leading to
302 the empirically most adequate results corresponds well to the findings of WSL (2017), indicating a reasonable degree
303 of plausibility. It remains equally difficult to quantify the amount of water injected into the rock avalanche by over-
304 load of the sediments and the resulting pore pressure rise. **The confirmation or rejection of conceptual models with
305 regard to the physical mechanisms involved in specific cases would have to be based on better constrained initial con-
306 ditions, and the availability of robust parameter sets.**

307 We note that with the approach chosen we are not able (i) to adequately simulate the transition from solid to fluid
308 material; and (ii) to consider rock and ice separately with different material properties, which would require a three-
309 phase model, not within the scope here. Therefore, entrained ice is considered viscous fluid from the beginning. A
310 physically better founded representation of the initial phase of the event would require an extension of the flow model
311 employed. Such an extension could build on the rock-ice avalanche model introduced by Pudasaini and Krautblatter
312 (2014). Also

313 the vertical patterns of the situation illustrated in **Fig. 5** cannot be modelled with the present approach, which (i) does
314 not consider melting of ice; and (ii) only allows one entrainable layer at each pixel. The assumption of fluid behaviour
315 of glacier ice therefore represents a necessary simplification which is supported by observations (Fig. 3b), but neglects
316 the likely presence of remaining ice in the basal part of the eroded glacier, which melted later and so contributed to
317 the successive debris flow surges. **Still, the Pudasaini (2012) model – and the extended multi-phase model (Pudasaini
318 and Mergili, 2019) – are currently considered best practice. Other two-phase or bulk mixture models, most notably the
319 approach presented by Iverson and George (2014) implemented in the software D-Claw, are less general and do not
320 consider the relative velocity between the phases, pore fluid diffusion, and interfacial momentum transfers at a com-
321 parable level, and are therefore less useful for the simulation of cascading effects.**

322 The initial rock slide-rock fall and the rock avalanche are simulated in a plausible way, at least with regard to the dep-
323 osition area. Whereas the simulated deposition area is clearly defined in **Scenario S2**, this is to a lesser extent the case
324 in **Scenario S1**, where the front of the rock avalanche directly transforms into a debris flow. Both scenarios seem to
325 overestimate the time between release and deposition, compared to the seismic signals recorded – an issue also report-
326 ed by WSL (2017) for their simulation. We observe a relatively gradual deceleration of the simulated avalanche, with-
327 out clearly defined stopping and note that also in the **Scenario S2**, there is some diffusion after the considered time of
328 120 s, so that the definition of the simulated deposit is somehow arbitrary. The elaboration of well-suited stopping
329 criteria, going beyond the very simple approach introduced by Mergili et al. (2017), remains a task for the future.
330 However, as the rock avalanche has already been successfully back-calculated by WSL (2017), we focus on the first
331 debris flow surge: the simulation input is optimized towards the back-calculation of the debris flow volumes entering

332 the valley at the hydrograph profile O2 (Table 3). The travel times to the hydrograph profiles O3 and O4 are repro-
333 duced in a plausible way in both scenarios, and so are the impact areas (Figs. 8 and 11). Exceedance of the lateral limits
334 in the lower zones is attributed to an overestimate of the debris flow volumes there, and to numerical issues related to
335 the narrow gorge. The same is true for the fan of Bondo. The solid ratio of the debris flow in the simulations appears
336 realistic, ranging around 40–45% in the early stage of the debris flow, and around 30–35% and lower (depending on
337 the cut-off time of the hydrograph) in the final stage. This means that solid material tends to stop in the transit area
338 rather than fluid material, as it can be expected. Nevertheless, the correct simulation of the deposition of debris flow
339 material along Val Bondasca remains a major challenge (Table 3). Even though a considerable amount of effort was put
340 in reproducing the much lower volumes reported in the vicinity of O4, the simulations result in an overestimate of the
341 volumes passing through this hydrograph profile. This is most likely a consequence of the failure of r.avaflow to ade-
342 quately reproduce the deposition pattern in the zones D and E. Whereas some material remains there at the end of the
343 simulation, more work is necessary to appropriately understand the mechanisms of deposition in viscous debris flows
344 (Pudasaini and Fischer, 2016b). Part of the discrepancy, however, might be explained by the fact that part of the fluid
345 material – which does not only consist of pure water, but of a mixture of water and fine mud – left the area of interest
346 in downstream direction and was therefore not included in the reference measurements.

347 The simulation results are strongly influenced by the initial conditions and the model parameters. Parameterization of
348 both scenarios is complex and highly uncertain, particularly in terms of optimizing the volumes of entrained till and
349 glacial meltwater, and injected pore water. In general, the parameter sets optimized to yield empirically adequate re-
350 sults are physically plausible, in contrast to Mergili et al. (2018b) who had to set the basal friction angle in a certain
351 zone to a negligible value in order to reproduce the observed overtopping of a more than 100 m high ridge (1970
352 Huascarán landslide). In contrast, reproducing the travel times to O4 in the present study requires the assumption of a
353 low mobility of the flow in Zone E. This is achieved by increasing the friction (Table 1), accounting for the narrow
354 flow channel, i.e. the interaction of the flow with the channel walls, which is not directly accounted for in r.avaflow.
355 Still, the high values of δ given in Table 1 are not directly applied, as they scale with the solid fraction. This type of
356 weighting has to be further scrutinized. We emphasize that also reasonable parameter sets are not necessarily physi-
357 cally true, as the large number of parameters involved (Tables 1 and 2) creates a lot of space for equifinality issues
358 (Beven et al., 1996).

359 We have further shown that the classical evaluation of empirical adequacy, by comparing observed and simulated
360 impact areas, is not enough in the case of complex mass flows: travel times, hydrographs, and volumes involved can
361 provide important insight in addition to the classical quantitative performance indicators used, for example, in land-
362 slide susceptibility modelling (Formetta et al., 2015). Further, the delineation of the observed impact area is uncertain
363 as the boundary of the event is not clearly defined particularly in Zone C.

364 The present work is seen as a further step towards a better understanding of the challenges and the parameterization
365 concerning the integrated simulation of complex mass flows. More case studies are necessary to derive guiding param-

366 eter sets facilitating predictive simulations of such events (Mergili et al., 2018a, b). A particular challenge of such case
367 studies consists in the parameter optimization procedure: in principle, automated methods do exist (e.g. Fischer, 2013).
368 However, they have been developed for optimizing globally defined parameters (which are constant over the entire
369 study area) against runout length and impact area, and such tools do a very good job for exactly this purpose. Howev-
370 er, they cannot directly deal with spatially variable parameters, as they are defined in the present work. With some
371 modifications they might even serve for that – but the main issue is that optimization also considers shapes and maxi-
372 mum values of hydrograph discharges, or travel times at different places of the path. It would be a huge effort to trim
373 optimization algorithms to this purpose, and to make them efficient enough to prevent excessive computational times
374 – we consider this as an important task for the future which is out of scope of the present work. Therefore, we have
375 used a step-wise expert-based optimization strategy.

376 7 Conclusions

377 Both of the investigated Scenarios S1 (debris flow developing at the front of the rock avalanche) and S2 (debris flow
378 developing at the back of the rock avalanche, overtopping the deposit) lead to empirically reasonable adequate results,
379 when back calculated with r.avaflow using physically plausible model parameters. Based on the simulations performed
380 in the present study, final conclusions on the more likely of the mechanisms sketched in Fig. 6 can therefore not be
381 drawn purely based on the simulations. The observed jet of glacial meltwater (Fig. 3b) points towards Scenario S1. The
382 observed scouring of the rock avalanche deposit, in contrast, rather points towards Scenario S2, but could also be asso-
383 ciated to subsequent debris flow surges. Open questions include at least (i) the interaction between the initial rock
384 slide-rock fall and the glacier; (ii) flow transformations in the lower portion of Zone C (Fig. 7), leading to the first de-
385bris flow surge; and (iii) the mechanisms of deposition of 90% of the debris flow material along the flow channel in
386 the Val Bondasca. Further research is therefore urgently needed to shed more light on this extraordinary landslide
387 cascade in the Swiss Alps. In addition, improved simulation concepts are needed to better capture the dynamics of
388 complex landslides in glacierized environments: such would particularly have to include three-phase models, where
389 ice – and melting of ice – are considered in a more explicit way. Finally, more case studies of complex mass flows have
390 to be performed in order to derive guiding parameter sets serving for predictive simulations.

391 Acknowledgements

392 Shiva P. Pudasaini gratefully thanks the Herbette Foundation for providing financial support for his sabbatical visit to
393 the University of Lausanne, Switzerland in the period April–June 2018, where this contribution was triggered. Simi-
394 larly, this work has been financially supported by the German Research Foundation (DFG) through the research pro-
395 ject PU 386/5-1: “A novel and unified solution to multi-phase mass flows”. It strongly builds on the outcomes of the
396 international cooperation project “A GIS simulation model for avalanche and debris flows (avaflow)” supported by the
397 German Research Foundation (DFG, project number PU 386/3-1) and the Austrian Science Fund (FWF, project num-
398 ber I 1600-N30).

399 We would like to thank Brian McArdell and another anonymous reviewer for providing constructive comments and
400 suggestions that helped to enhance the paper substantially, and are grateful to Sophia Demmel and Florian Amann for
401 valuable discussions and to Matthias Benedikt for comprehensive technical assistance.

402 **References**

- 403 Amann, F., Kos, A., Phillips, M., and Kenner, R.: The Piz Cengalo Bergsturz and subsequent debris flows, *Geophys.*
404 *Res. Abstr.*, 20, 14700, 2018.
- 405 Amt für Wald und Naturgefahren: Bondo: Chronologie der Ereignisse, 2 pp.,
406 https://www.gr.ch/DE/institutionen/verwaltung/bvfd/awn/dokumentenliste_afw/20170828_Chronologie_Bondo_2017_12_13_dt.pdf, accessed on 31 May 2019.
- 408 Beven, K.: Equifinality and Uncertainty in Geomorphological Modelling, in: *The Scientific Nature of Geomorphology: Proceedings of the 27th Binghamton Symposium in Geomorphology, 27-29 September 1996*, John Wiley & Sons, 289–
409 313, 1996.
- 411 Bonanomi, Y., and Keiser, M.: Bericht zum aktuellen Bergsturz am Piz Cengalo 2017, Bergeller Alpen im Engadin, 19.
412 Geoforum Umhausen, 19.–20. Oktober 2017, 55–60, 2017.
- 413 Christen, M., Kowalski, J., and Bartelt, P.: RAMMS: Numerical simulation of dense snow avalanches in three-
414 dimensional terrain, *Cold Reg. Sci. Technol.*, 63, 1–14, <https://doi.org/10.1016/j.coldregions.2010.04.005>, 2010.
- 415 De Blasio, F. V., and Crosta, G. B.: Extremely Energetic Rockfalls: Some preliminary estimates, in: *Landslides and Engineered Slopes. Experience, Theory and Practice*, 759–764, CRC Press, 2016.
- 417 Demmel, S.: Water Balance in Val Bondasca. Initial hydrological conditions for debris flows triggered by the 2017 rock
418 avalanche at Pizzo Cengalo. Master Thesis, ETH Zurich, 50 pp., 2019.
- 419 Domnik, B., Pudasaini, S. P., Katzenbach, R., and Miller, S. A.: Coupling of full two-dimensional and depth-averaged
420 models for granular flows, *J. Non-Newtonian Fluid Mech.*, 201, 56–68, <https://doi.org/10.1016/j.jnnfm.2013.07.005>,
421 2013.
- 422 Evans, S. G., Bishop, N.F., Fidel Smoll, L., Valderrama Murillo, P., Delaney, K.B., and Oliver-Smith, A.: A re-
423 examination of the mechanism and human impact of catastrophic mass flows originating on Nevado Huascarán, Cor-
424 dillera Blanca, Peru in 1962 and 1970, *Eng. Geol.*, 108, 96–118, <https://doi.org/10.1016/j.enggeo.2009.06.020>, 2009.
- 425 Fischer, J.-T., Kowalski, J., and Pudasaini, S. P.: Topographic curvature effects in applied avalanche modeling, *Cold*
426 *Reg. Sci. Technol.*, 74, 21–30, <https://doi.org/10.1016/j.coldregions.2012.01.005>, 2012.
- 427 Fischer, J.-T., Kofler, A., Fellin, W., Granig, M., and Kleemayr, K.: Multivariate parameter optimization for computa-
428 tional snow avalanche simulation in 3d terrain, *J. Glaciol.*, 61(229), 875–888, <https://doi.org/10.3189/2015JoG14J168>,
429 2015.

430 Formetta, G., Capparelli, G., and Versace, P.: Evaluating performances of simplified physically based models for land-
431 slide susceptibility, *Hydrol. Earth Syst. Sci. Discuss.*, 12, 13217–13256, <https://doi.org/10.5194/hessd-19-1-2015>, 2015.

432 Frank, F., Huggel, C., McArdeell, B. W., and Vieli, A.: Landslides and increased debris-flow activity: a systematic com-
433 parison of six catchments in Switzerland. *Earth Surf. Proc. Landforms*, 44(3), 699–712,
434 <https://doi.org/10.1002/esp.4524>, 2019.

435 Haeberli, W.: Mountain permafrost—research frontiers and a special long-term challenge, *Cold Reg. Sci. Technol.*, 96,
436 71–76, <https://doi.org/10.1016/j.coldregions.2013.02.004>, 2013.

437 Haeberli, W., and Whiteman, C. (Eds.): *Snow and Ice-related Hazards, Risks and Disasters*, Elsevier,
438 <https://doi.org/10.1016/B978-0-12-394849-6.00001-9>, 2014.

439 Haeberli, W., Schaub, Y., and Huggel, C.: Increasing risks related to landslides from degrading permafrost into new
440 lakes in de-glaciating mountain ranges, *Geomorphology*, 293(B), 405–417,
441 <https://doi.org/10.1016/j.geomorph.2016.02.009>, 2017.

442 Harris, C., Arenson, L. U., Christiansen, H. H., Etzelmüller, B., Frauenfelder, R., Gruber, S., Haeberli, W., Hauck, C.,
443 Hölzle, M., Humlum, O., Isaksen, K., Käab, A., Kern-Lütschg, M. A., Lehning, M., Matsuoka, N., Murton, J. B., Nötzli,
444 J., Phillips, M., Ross, N., Seppälä, M., Springman, S. M., and Vonder Mühll, D.: Permafrost and climate in Europe:
445 Monitoring and modelling thermal, geomorphological and geotechnical responses, *Earth-Sci. Rev.*, 92, 117–171,
446 <https://doi.org/10.1016/j.earscirev.2008.12.002>, 2009.

447 Hewitt, K.: Styles of rock-avalanche depositional complexes conditioned by very rugged terrain, Karakoram Himalaya,
448 *Pakistan, Rev. Eng. Geol.*, 15, 345–377, 2002.

449 Huggel, C., Zraggen-Oswald, S., Haeberli, W., Käab, A., Polkvoj, A., Galushkin, I., and Evans, S.G.: The 2002 rock/ice
450 avalanche at Kolka/Karmadon, Russian Caucasus: assessment of extraordinary avalanche formation and mobility, and
451 application of QuickBird satellite imagery, *Nat. Hazards Earth Syst. Sci.*, 5, 173–187, [https://doi.org/10.5194/nhess-5-](https://doi.org/10.5194/nhess-5-173-2005)
452 173-2005, 2005.

453 Iverson, R. M.: The physics of debris flows, *Rev. Geophys.*, 35, 245–296, <https://doi.org/10.1029/97RG00426>, 1997.

454 Kattel, P., Khattri, K. B., Pokhrel, P. R., Kafle, J., Tuladhar, B. M., and Pudasaini, S. P.: Simulating glacial lake outburst
455 floods with a two-phase mass flow model, *Ann. Glaciol.*, 57(71), 349–358, <https://doi.org/10.3189/2016AoG71A039>,
456 2016.

457 Krautblatter, M., Funk, D., and Günzel, F. K.: Why permafrost rocks become unstable: a rock–ice–mechanical model
458 in time and space, *Earth Surf. Process. Landf.*, 38, 876–887, <https://doi.org/10.1002/esp.3374>, 2013.

459 McDougall, S., and Hungr, O.: A Model for the Analysis of Rapid Landslide Motion across Three-Dimensional Terrain,
460 *Can. Geotech. J.*, 41, 1084–1097, <https://doi.org/10.1139/t04-052>, 2004.

461 Mergili, M., Pudasaini, S. P.: r.avaflow – The open source mass flow simulation model, <https://www.avaflow.org/>, last
462 access: 7 July 2019.

463 Mergili, M., Fischer, J.-T., Krenn, J., and Pudasaini, S. P.: r.avaflow v1, an advanced open source computational
464 framework for the propagation and interaction of two-phase mass flows, *Geosci. Model Dev.*, 10, 553–569,
465 <https://doi.org/10.5194/gmd-10-553-2017>, 2017.

466 Mergili, M., Emmer, A., Juřicová, A., Cochachin, A., Fischer, J.-T., Huggel, C., and Pudasaini, S.P.: How well can we
467 simulate complex hydro-geomorphic process chains? The 2012 multi-lake outburst flood in the Santa Cruz Valley
468 (Cordillera Blanca, Perú), *Earth Surf. Process. Landf.*, 43(7), 1373–1389, <https://doi.org/10.1002/esp.4318>, 2018a.

469 Mergili, M., Frank, B., Fischer, J.-T., Huggel, C., and Pudasaini, S. P.: Computational experiments on the 1962 and
470 1970 landslide events at Huascarán (Peru) with r.avaflow: Lessons learned for predictive mass flow simulations, *Geo-*
471 *morphology*, 322, 15–28, <https://doi.org/10.1016/j.geomorph.2018.08.032>, 2018b.

472 Nesyahu, H., and Tadmor, E.: Non-oscillatory central differencing for hyperbolic conservation laws, *J. Comput.*
473 *Phys.*, 87, 408–463, [https://doi.org/10.1016/0021-9991\(90\)90260-8](https://doi.org/10.1016/0021-9991(90)90260-8), 1990.

474 Nicoletti, G. P., and Sorriso-Valvo, M.: Geomorphic controls of the shape and mobility of rock avalanches, *GSA Bull.*,
475 103(10), 1365–1373, [https://doi.org/10.1130/0016-7606\(1991\)103<1365:GCOTSA>2.3.CO;2](https://doi.org/10.1130/0016-7606(1991)103<1365:GCOTSA>2.3.CO;2), 1991.

476 Pitman, E.B., and Le, L.: A two-fluid model for avalanche and debris flows. *Philos. Trans. R. Soc. A*, 363, 1573–1601,
477 <https://doi.org/10.1098/rsta.2005.1596>, 2005.

478 Pudasaini, S. P.: A general two-phase debris flow model, *J. Geophys. Res. Earth Surf.*, 117, F03010,
479 <https://doi.org/10.1029/2011JF002186>, 2012.

480 Pudasaini, S. P.: A full description of generalized drag in mixture mass flows, *Phys. Fluids*, submitted manuscript,
481 2019.

482 Pudasaini, S. P., and Krautblatter, M.: A two-phase mechanical model for rock-ice avalanches, *J. Geophys. Res. Earth*
483 *Surf.*, 119, doi:10.1002/2014JF003183, 2014.

484 Pudasaini, S. P., and Fischer, J.-T.: A mechanical model for phase-separation in debris flow, arXiv:1610.03649, 2016a.

485 Pudasaini, S.P., and Fischer, J.-T.: A mechanical erosion model for two-phase mass flows, arXiv:1610.01806, 2016b.

486 Pudasaini, S.P., and Mergili, M.: A Multi-Phase Mass Flow Model, *J. Geophys. Res. Earth Surf.*, JGRF21102,
487 <https://doi.org/10.1029/2019JF005204>, 2019.

488 Preh, A., and Sausgruber, J. T.: The Extraordinary Rock-Snow Avalanche of Alpl, Tyrol, Austria. Is it Possible to Pre-
489 dict the Runout by Means of Single-phase Voellmy- or Coulomb-Type Models?, in: *Engineering Geology for Society*
490 *and Territory–Volume 2*, edited by: Lollino, G. et al., Springer, Cham, https://doi.org/10.1007/978-3-319-09057-3_338,
491 2015.

492 Saltelli, A., and Annoni, P.: How to avoid a perfunctory sensitivity analysis, *Environ. Model. Softw.*, 25, 1508–1517,
493 <https://doi.org/10.1016/j.envsoft.2010.04.012>, 2010.

494 Savage, S. B., and Hutter, K.: The motion of a finite mass of granular material down a rough incline, *J. Fluid Mech.*,
495 199, 177–215, <https://doi.org/10.1017/S0022112089000340>, 1989.

496 Scheidegger, A. E.: On the Prediction of the Reach and Velocity of Catastrophic Landslides, *Rock Mech.*, 5, 231–236,
497 <https://doi.org/10.1007/BF01301796>, 1973.

498 Schneider, D., Huggel, C., Cochachin, A., Guillén, S., and García, J.: Mapping hazards from glacier lake outburst floods
499 based on modelling of process cascades at Lake 513, Carhuaz, Peru, *Adv. Geosci.*, 35, 145–155,
500 <https://doi.org/10.5194/adgeo-35-145-2014>, 2014.

501 Somos-Valenzuela, M. A., Chisolm, R. E., Rivas, D. S., Portocarrero, C., and McKinney, D. C.: Modeling a glacial lake
502 outburst flood process chain: the case of Lake Palcacocha and Huaraz, Peru, *Hydrol. Earth Syst. Sci.*, 20, 2519–2543,
503 <https://doi.org/10.5194/hess-20-2519-2016>, 2016.

504 Steinacher, R., Kuster, C., Buchli, C., and Meier, L.: The Pizzo Cengalo and Val Bondasca events: From early warnings
505 to immediate alarms, *Geophys. Res. Abstr.* 20, 17536, 2018.

506 Tai, Y. C., Noelle, S., Gray, J. M. N. T., and Hutter, K.: Shock-capturing and front-tracking methods for granular ava-
507 lanches, *J. Comput. Phys.*, 175(1), 269–301, <https://doi.org/10.1006/jcph.2001.6946>, 2002.

508 VAW: Vadrec dal Cengal Ost: Veränderungen in Vergangenheit und Zukunft. Laboratory of Hydraulics, Hydrology
509 and Glaciology of the Swiss Federal Institute of Technology Zurich, 17 pp.,
510 [https://www.gr.ch/DE/institutionen/verwaltung/bvfd/awn/dokumentenliste_afw/Cengalo%20Gletscherentwicklung%
511 20ETH_2nov_final.pdf](https://www.gr.ch/DE/institutionen/verwaltung/bvfd/awn/dokumentenliste_afw/Cengalo%20Gletscherentwicklung%20ETH_2nov_final.pdf), accessed on 31 May 2019, 2017.

512 Voellmy, A.: Über die Zerstörungskraft von Lawinen, *Schweizerische Bauzeitung*, 73, 159–162, 212–217, 246–249,
513 280–285, 1955.

514 Walter, F., Wenner, M., and Amann, F.: Seismic Analysis of the August 2017 Landslide on Piz Cengalo (Switzerland),
515 *Geophys. Res. Abstr.*, 20, 3163-1, 2018.

516 Walter, F., Amann, F., Kos, A., Kenner, R., Phillips, M., de Preux, A., Huss, M., Tognacca, C., Clinton, J., Diehl, T., and
517 Bonanomi, Y.: Direct observations of a three million cubic meter rock-slope collapse with almost immediate initiation
518 of ensuing debris flows, *Earth Planet. Sci. Lett.*, submitted manuscript, 2019.

519 Wang, Y., Hutter, K., and Pudasaini, S. P.: The Savage-Hutter theory: A system of partial differential equations for
520 avalanche flows of snow, debris, and mud, *ZAMM – J. Appl. Math. Mech.*, 84(8), 507–527,
521 <https://doi.org/10.1002/zamm.200310123>, 2004.

522 Worni, R., Huggel, C., Clague, J. J., Schaub, Y., and Stoffel, M.: Coupling glacial lake impact, dam breach, and flood
523 processes: A modeling perspective, *Geomorphology*, 224, 161–176, <https://doi.org/10.1016/j.geomorph.2014.06.031>,
524 2014.

525 WSL.: SLF Gutachten G2017.20: Modellierung des Cengalo Bergsturzes mit verschiedenen Rahmenbedingungen, Bon-
526 do, GR. WSL-Institut für Schnee- und Lawinenforschung SLF, 69 pp.,
527 [https://www.gr.ch/DE/institutionen/verwaltung/bvfd/awn/dokumentenliste_afw/SLF_G2017_20_Modellierung_Cenga](https://www.gr.ch/DE/institutionen/verwaltung/bvfd/awn/dokumentenliste_afw/SLF_G2017_20_Modellierung_Cengalo_Bergsturz_030418_A.pdf)
528 [lo_Bergsturz_030418_A.pdf](https://www.gr.ch/DE/institutionen/verwaltung/bvfd/awn/dokumentenliste_afw/SLF_G2017_20_Modellierung_Cengalo_Bergsturz_030418_A.pdf), accessed on 31 May 2019, 2017.

529

531 Table 1. Descriptions and optimized parameter values for each of the zones A–F (Fig. 4 and Fig. 7). The names of the
 532 model parameters are given in the text and in Table 2. The values provided in Table 2 are assigned to those parameters
 533 not shown. (S1) and (S2) refer to the corresponding scenarios.

Zone	Description	Model parameters	Initial conditions
A	Rock zone – NE face of Piz Cengalo with rock slide-rock fall release area	$\delta = 20^\circ$ (S1) ¹⁾ $\delta = 13^\circ$ (S2) ²⁾ $C_{AD} = 0.2$	Release volume: 3.2 million m ³ , 100 % solid ³⁾
B	Glacier zone – Cirque glacier beneath zone A, entrainment of glacier ice ¹⁾	$\delta = 20^\circ$ (S1) $\delta = 13^\circ$ (S2) $C_E = 10^{-6.5}$	Entrainment of glacier ice and till (Table 3) ⁴⁾
C	Slope zone – steep, partly debris-covered glacier forefield leading down to the Val Bondasca	$\delta = 20^\circ$ (S1) $\delta = 13^\circ$ (S2) $C_E = 10^{-6.5}$ (S1) $C_E = 10^{-8.0}$ (S2)	Entrainment of injected water in Scenario S1 Entrainment of rock avalanche deposit in Scenario S2
D	Upper Val Bondasca zone – clearly defined flow channel becoming narrower in downstream direction	$\delta = 20-45^\circ$	No entrainment allowed, increasing friction
E	Lower Val Bondasca zone – narrow gorge	$\delta = 45^\circ$ $C_{FF} = 0.5$	No entrainment allowed, high friction due to lateral confinement
F	Bondo zone – deposition of the debris flow on the cone of Bondo	$\delta = 20^\circ$	No entrainment allowed

534 ¹⁾ Note that in all zones and in both of the scenarios S1 and S2, δ is assumed to scale linearly with the solid fraction.
 535 This means that the values given only apply in case of 100% solid.

536 ²⁾ This only applies to the initial landslide, which is assumed completely dry in Scenario S2. Due to the scaling of δ
 537 with the solid fraction, a lower basal friction is required to obtain results similar to Scenario S1, where the rock ava-
 538 lanche contains some fluid. The same values of δ as for Scenario S1 are applied for the debris flow in Scenario S2
 539 throughout all zones.

540 ³⁾ This volume is derived from our own reconstruction (Fig. 5). In contrast, WSL (2017) gives 3.1 million m³, and
 541 Amann et al. (2018) 3.15 million m³.

542 ⁴⁾ In Scenario S2, the glacier is not directly entrained, but instead released behind the rock avalanche. In both scenarios,
 543 ice is considered to melt immediately on impact and included in the viscous fluid fraction. See text for more de-
 544 tailed explanations.

545

546 Table 2. Model parameters used for the simulations.

Symbol	Parameter	Unit	Value
ρ_S	Solid material density (grain density)	kg m ⁻³	2,700
ρ_F	Fluid material density	kg m ⁻³	1,400 ¹⁾
φ	Internal friction angle	Degree	27 ²⁾
δ	Basal friction angle	Degree	Table 1
ν	Kinematic viscosity of the fluid	m ² s ⁻¹	10
τ_Y	Yield strength of the fluid	Pa	10
C_{AD}	Ambient drag coefficient	–	0.04 (exceptions in Table 1)
C_{FF}	Fluid friction coefficient	–	0.0 (exceptions in Table 1)
C_E	Entrainment coefficient	–	Table 1

547 ¹⁾ Fluid is here considered as a mixture of water and fine particles. This explains the higher density, compared to pure
548 water.

549 ²⁾ The internal friction angle φ always has to be larger than or equal to the basal friction angle δ . Therefore, in case of
550 $\delta > \varphi$, φ is increased accordingly.

551

552 Table 3. Selected output parameters of the simulations for the Scenarios S1 and S2 compared to the observed or docu-
 553 mented parameter values. S = solid; F = fluid; fractions are expressed in terms of volume; t_0 = time from the initial re-
 554 lease to the release of the first debris flow surge. Reference values are extracted from Amt für Wald und Naturgefah-
 555 ren (2017a), Bonanomi and Keiser (2017), and WSL (2017). *** = empirically adequate (within the documented range of
 556 values); ** = empirically partly adequate (less than 50% away from the documented range of values); * = empirically
 557 inadequate (at least 50% away from the documented range of values). The arithmetic means of minimum and maxi-
 558 mum of each range are used for the calculations.

Parameter	Documenta- tion/Observation	Scenario S1	Scenario S2
Entrained ice (m ³)	600,000 ¹⁾	–	–
Entrained S (m ³)	–	60,000	60,000 ²⁾
Entrained F (m ³)	–	305,000	240,000
Duration of initial landslide (s)	60–90 ³⁾	100–120**	100–120**
Travel time to O2 (s)	90–120 ⁴⁾	140**	t_0+120 ***
Travel time to O3 (s)	210–300 ⁵⁾	280***	t_0+240 ***
Travel time to O4 (s)	630–1020 ⁶⁾	700***	t_0+640 ***
Debris flow volume at O2 (m ³)	540,000	530,000** (43% S)	430,000** (45% S)
Debris flow volume at O4 (m ³)	50,000	265,000* (34% S)	270,000* (24% S)

559 ¹⁾ Not all the material entrained from the glacier was relevant for the first debris flow surge (Fig. 6), therefore lower
 560 volumes of entrained S (coarse till, in Scenario S2 also rock avalanche deposit) and F (molten ice and fine till, in Sce-
 561 nario S1 also pore water) yield the empirically most adequate results. The F volumes originating from the glacier in the
 562 simulations represent approx. half of the water equivalent of the entrained ice, corresponding well to the findings of
 563 WSL (2017).

564 ²⁾ This value does not include the 145,000 m³ of solid material remobilized through entrainment from the rock ava-
 565 lanche deposit in Scenario S2.

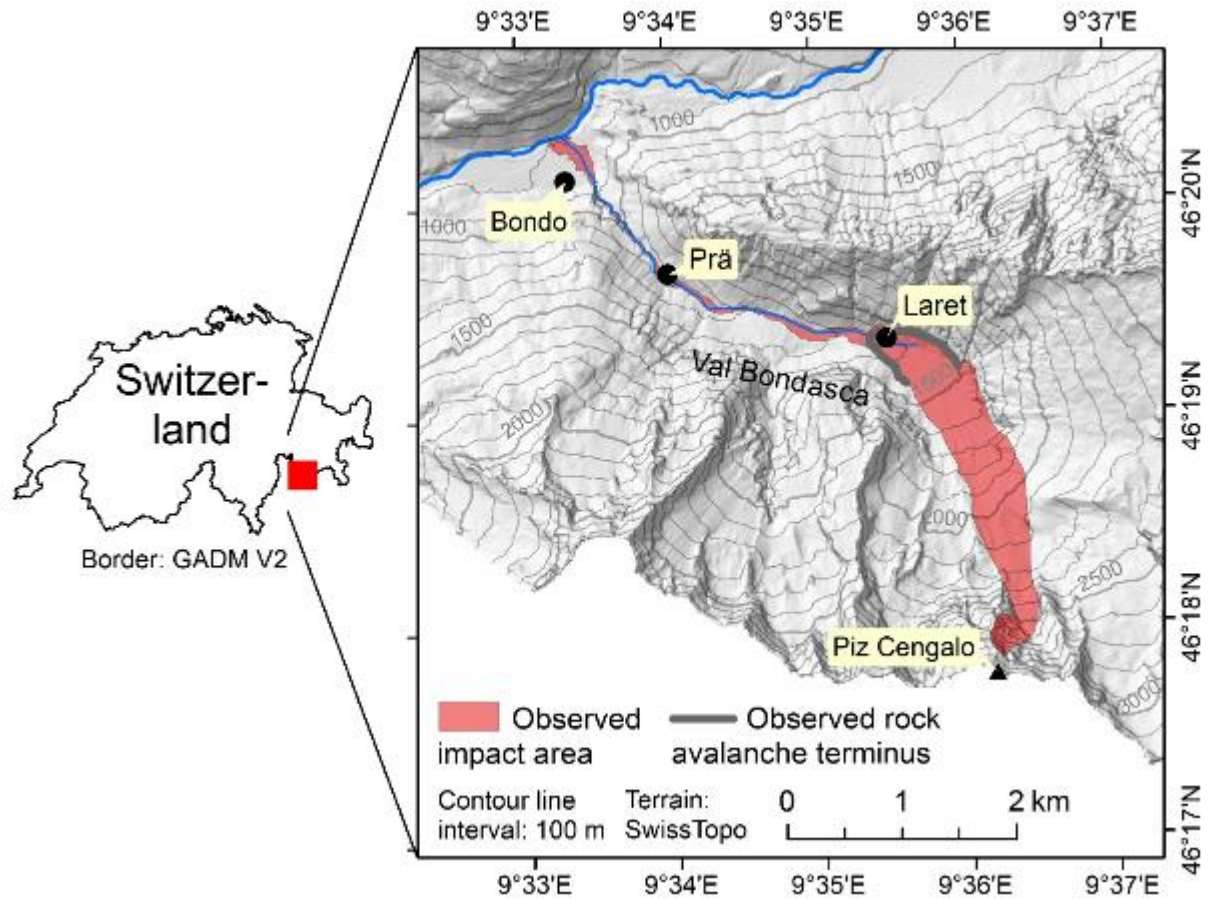
566 ³⁾ WSL (2017) states that the rock avalanche came to rest approx. 60 s after release, whereas the seismic signals ceased
 567 90 s after release.

568 ⁴⁾ A certain time (here, we assume a maximum of 30 s) has to be allowed for the initial debris flow surge to reach O2,
 569 located slightly downstream of the front of the rock avalanche deposit.

570 ⁵⁾ WSL (2017) gives a travel time of 3.5 minutes to Prä, roughly corresponding to the location of O3. It remains unclear
 571 whether this number refers to the release of the initial rock slide-rock fall or (more likely) to the start of the first de-
 572bris flow surge. Bonanomi and Keiser (2017) give a travel time of roughly four minutes between the initial release and
 573 the arrival of the first surge at the sensor of Prä.

574 ⁶⁾ Amt für Wald und Naturgefahren (2017) gives a time span of 17 minutes between the release of the initial rock
 575 slide-rock fall and the arrival of the first debris flow surge at the “bridge” in Bondo. However, it is not indicated to
 576 which bridge this number refers. WSL (2017), in contrast, give a travel time of 7–8 minutes from Prä to the “old
 577 bridge” in Bondo, which, in sum, results in a shorter total travel time as indicated in Amt für Wald und Naturgefahren
 578 (2017). Depending on the bridge, the reference location for these numbers might be downstream from O4. In the sim-
 579 ulation, this hydrograph shows a slow onset – travel times refer to the point when 5% of the total peak discharge are
 580 reached.

581



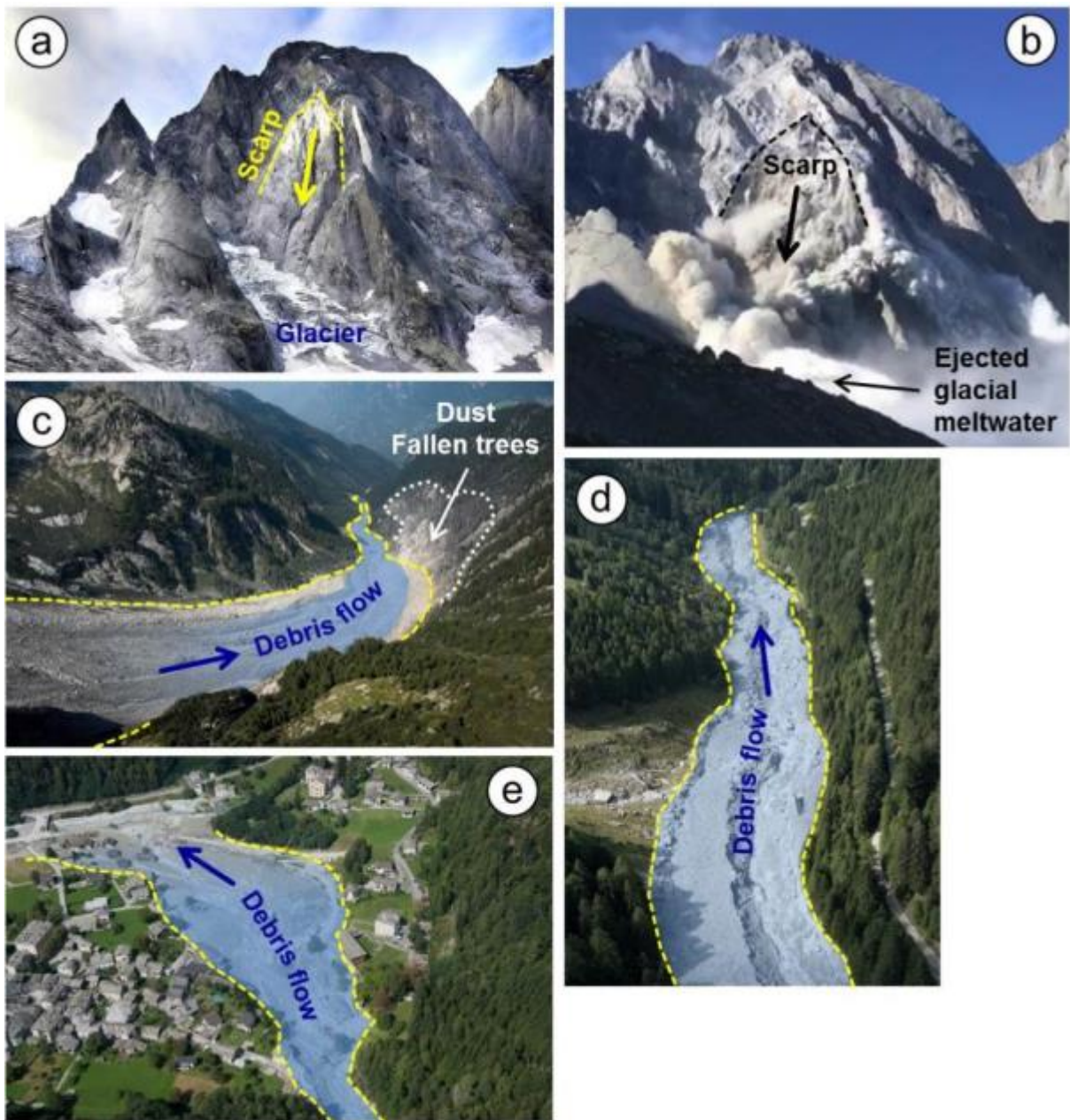
583
584
585
586

Figure 1. Study area with the impact area of the 2017 Piz Cengalo-Bondo landslide cascade. The observed rock avalanche terminus was derived from WSL (2017).



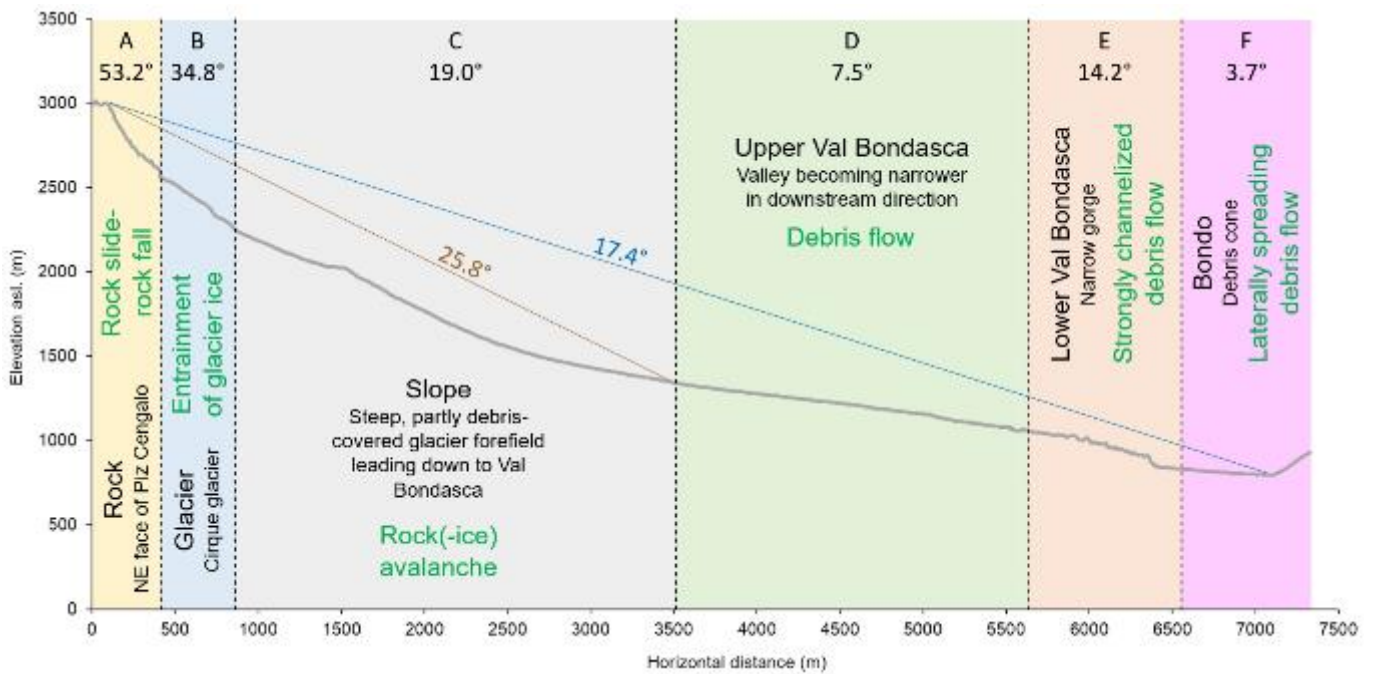
587
588
589
590

Figure 2. Oblique view of the impact area of the event, orthophoto draped over the 2011 DTM. Data sources: swisstopo.



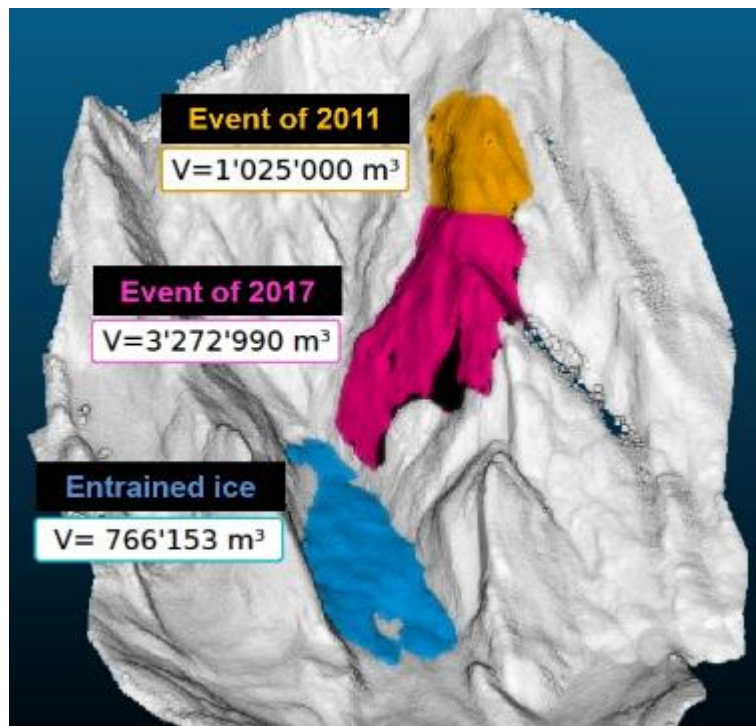
591
592
593
594
595
596
597
598

Figure 3. The 2017 Piz Cengalo-Bondo landslide cascade. (a) Scarp area on 20 September 2014. (b) Scarp area on 23 September 2017 at 9:30, 20 s after release, frame of a video taken from the Capanna di Sciora. Note the fountain of water and/or crushed ice at the front of the avalanche, most likely representing meltwater from the impacted glacier. (c) Upper part of the Val Bondasca, where the channelized debris flow developed. Note the zone of dust and pressure-induced damages to trees on the right side of the valley. (d) Traces of the debris flows in the Val Bondasca. (e) The debris cone of Bondo after the event. Image sources: Daniele Porro (a), Diego Salasc (b), VBS swisstopo Flugdienst (c)–(e).



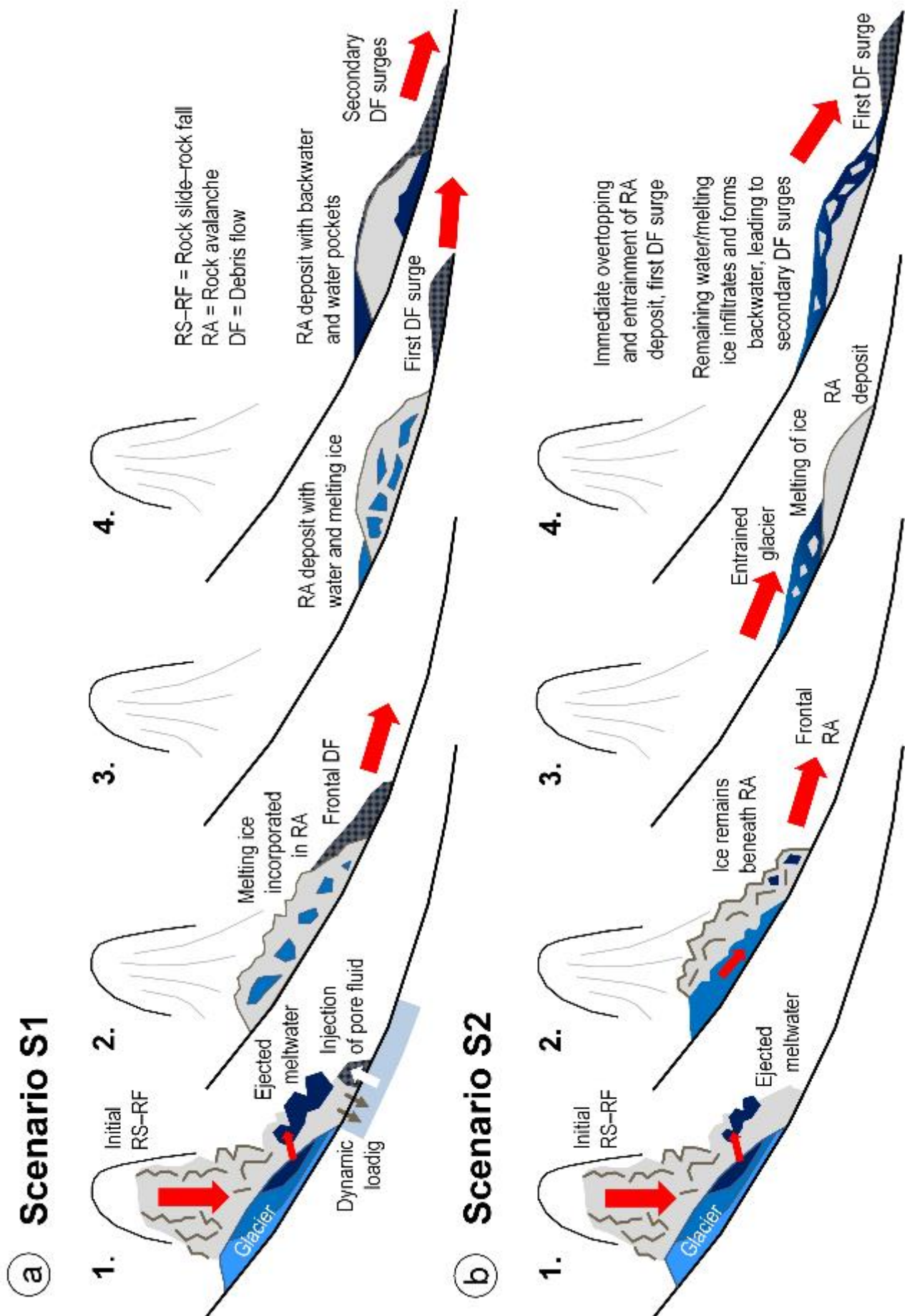
599
600
601
602
603
604
605

Figure 4. Profile along the main flow path of the Piz Cengalo-Bondo landslide cascade. The letters A–F indicate the individual zones (Table 1 and Fig. 7), whereas the associated numbers indicate the average angles of reach along the profile for each zone. The brown number and line show the angle of reach of the initial landslide (rock slide-rock fall and rock(-ice) avalanche), whereas the blue number and line show the angle of reach of the entire landslide cascade. The geomorphic characteristics of the zone (in black) are indicated along with the dominant process type (in green).

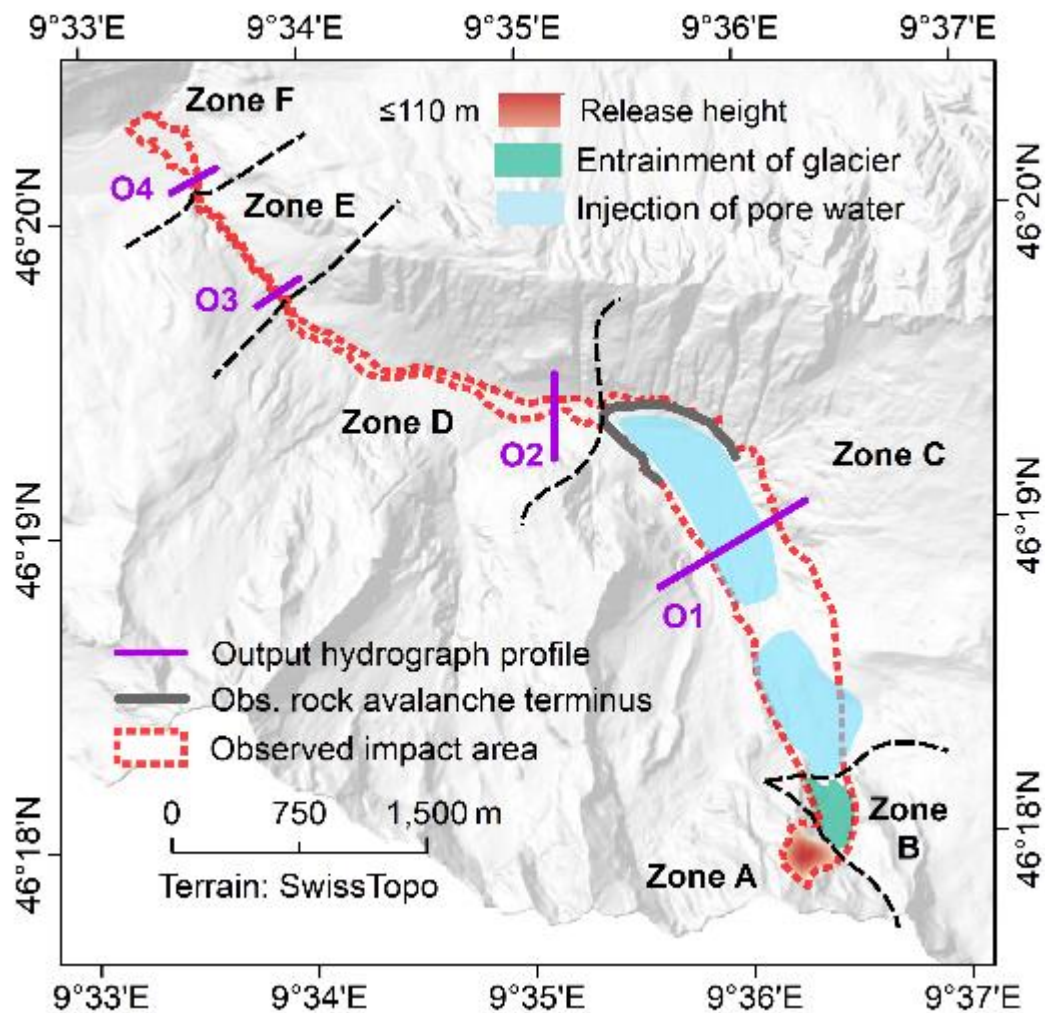


606
 607
 608
 609
 610
 611

Figure 5. Reconstruction of the released rock volume and the entrained glacier volume in the 2017 Piz Cengalo-Bondo landslide cascade. Note that the boundary between the 2011 and 2017 release volumes is connected to some uncertainties, explaining the slight discrepancies among the reported volumes. The glacier volume shown is neither corrected for entrainment related to the 2011 event, nor for glacier retreat in the period 2011–2017.

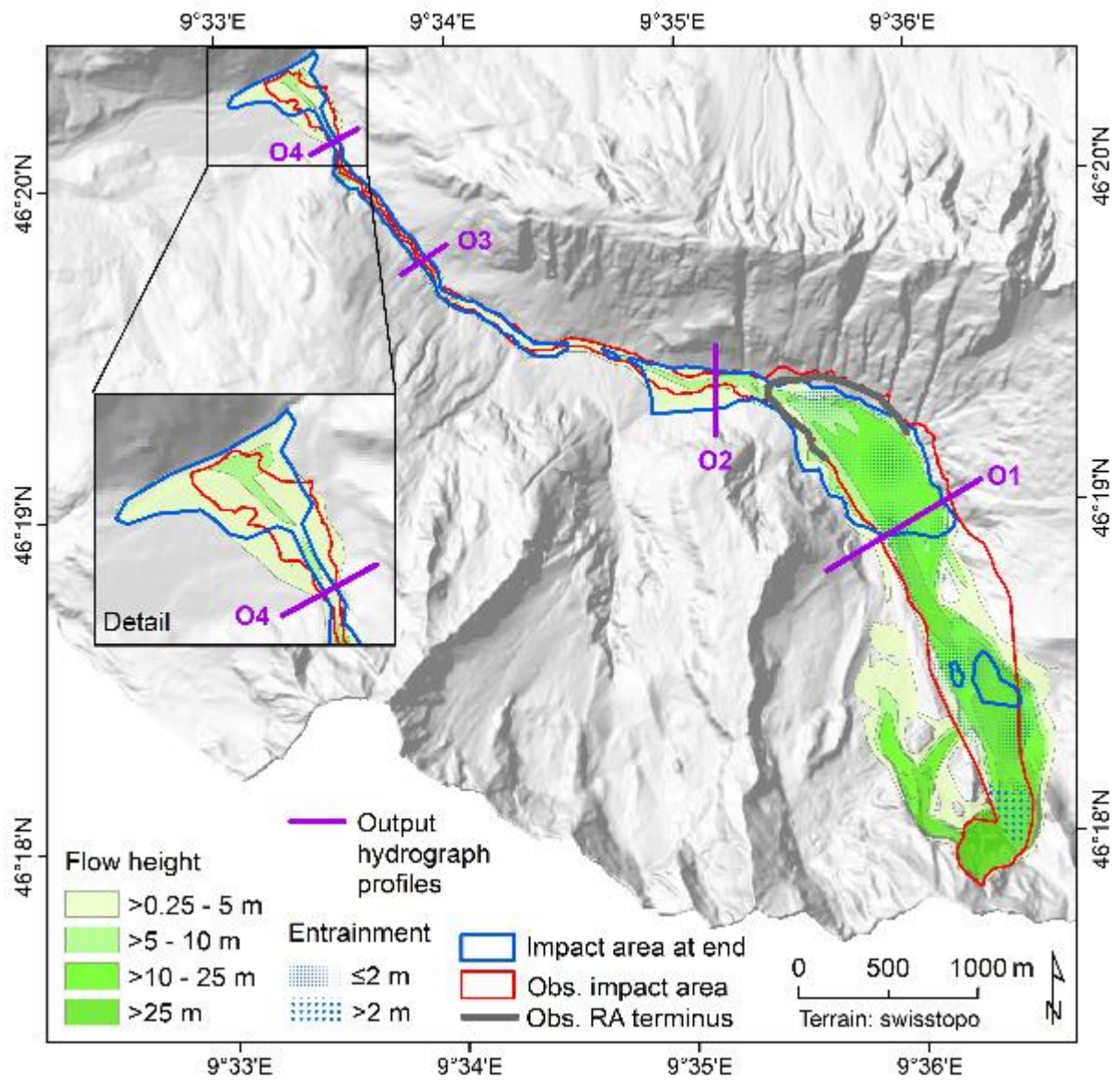


612
 613 **Figure 6.** Qualitative conceptual models of the rock avalanche-debris flow transformation. (a) **Scenario S1**; (b) **Scenario**
 614 **S2.** See text for the detailed description of the two scenarios.
 615

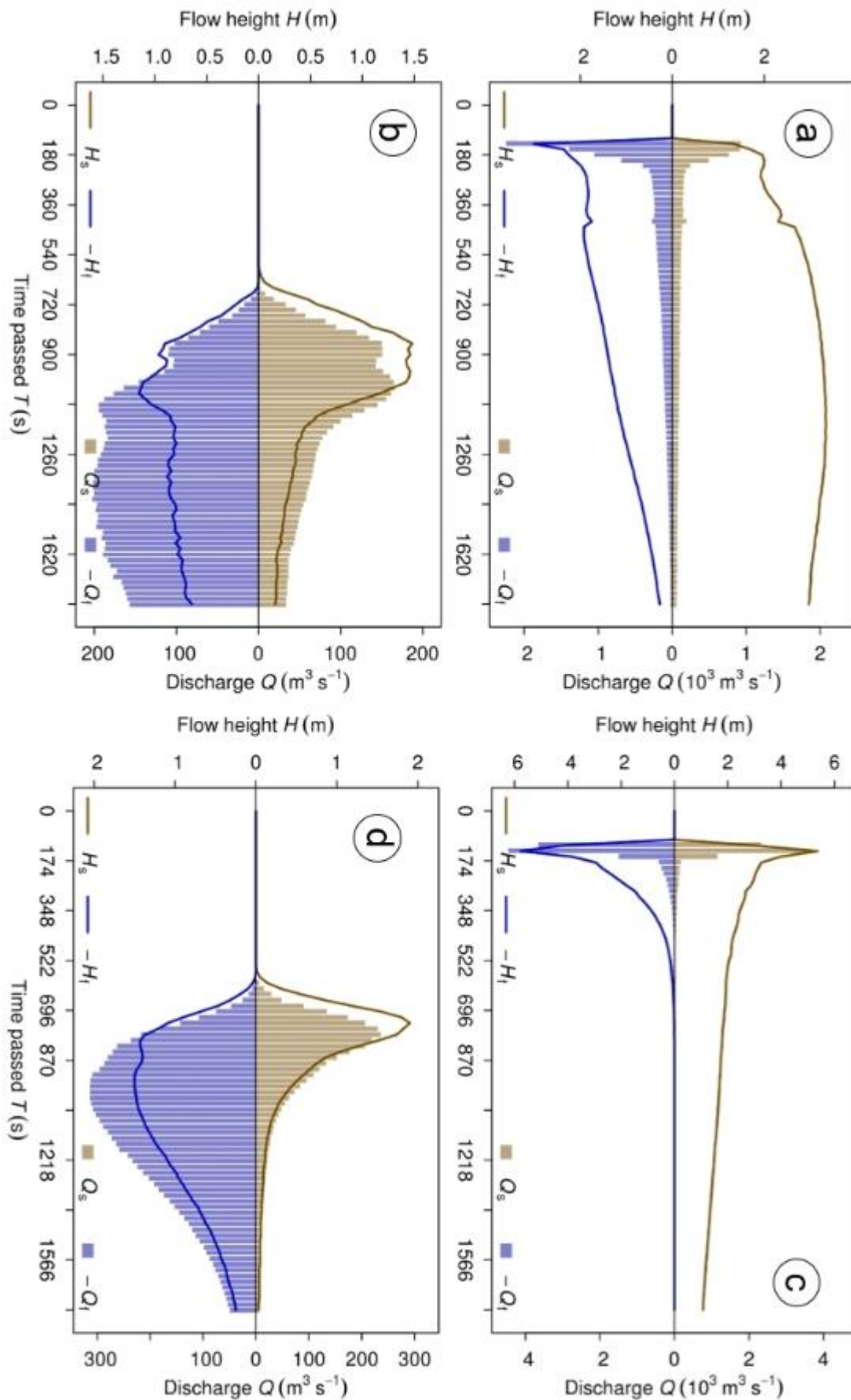


616
617
618
619
620
621
622

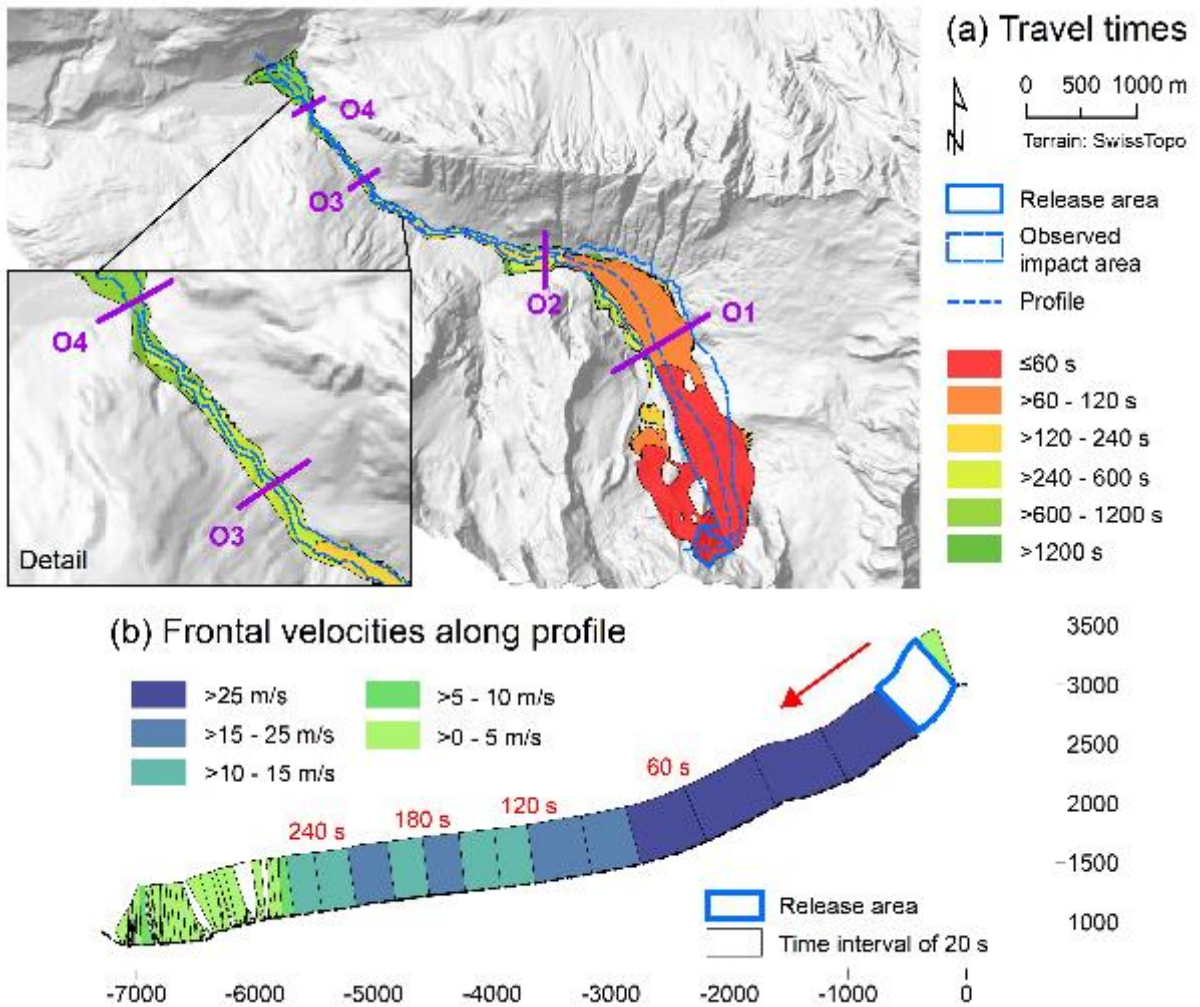
Figure 7. Overview of the heights and entrainment areas as well as the zonation performed as the basis for the simulation with r.avaflow. Injection of pore water only applies to the Scenario A. The zones A–F represent areas with largely homogeneous surface characteristics. The characteristics of the zones and the model parameters associated to each zone are summarized in Table 1 and Fig. 4. O1–O4 represent the output hydrograph profiles. The observed rock avalanche terminus was derived from WSL (2017).



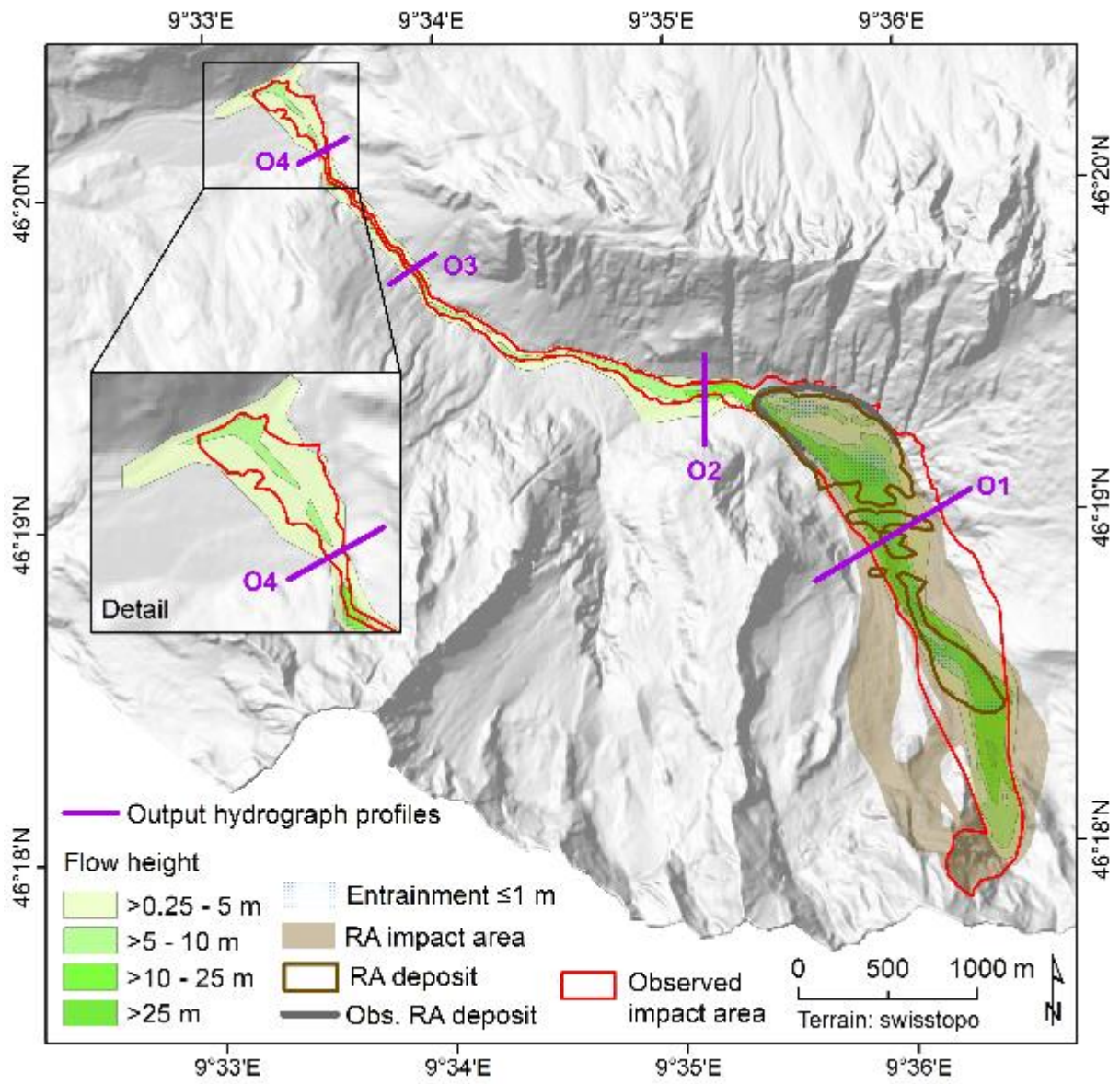
623 **Figure 8.** Maximum flow height and entrainment derived for **Scenario S1**. RA = rock avalanche; the observed RA ter-
 624 minus was derived from WSL (2017).
 625
 626



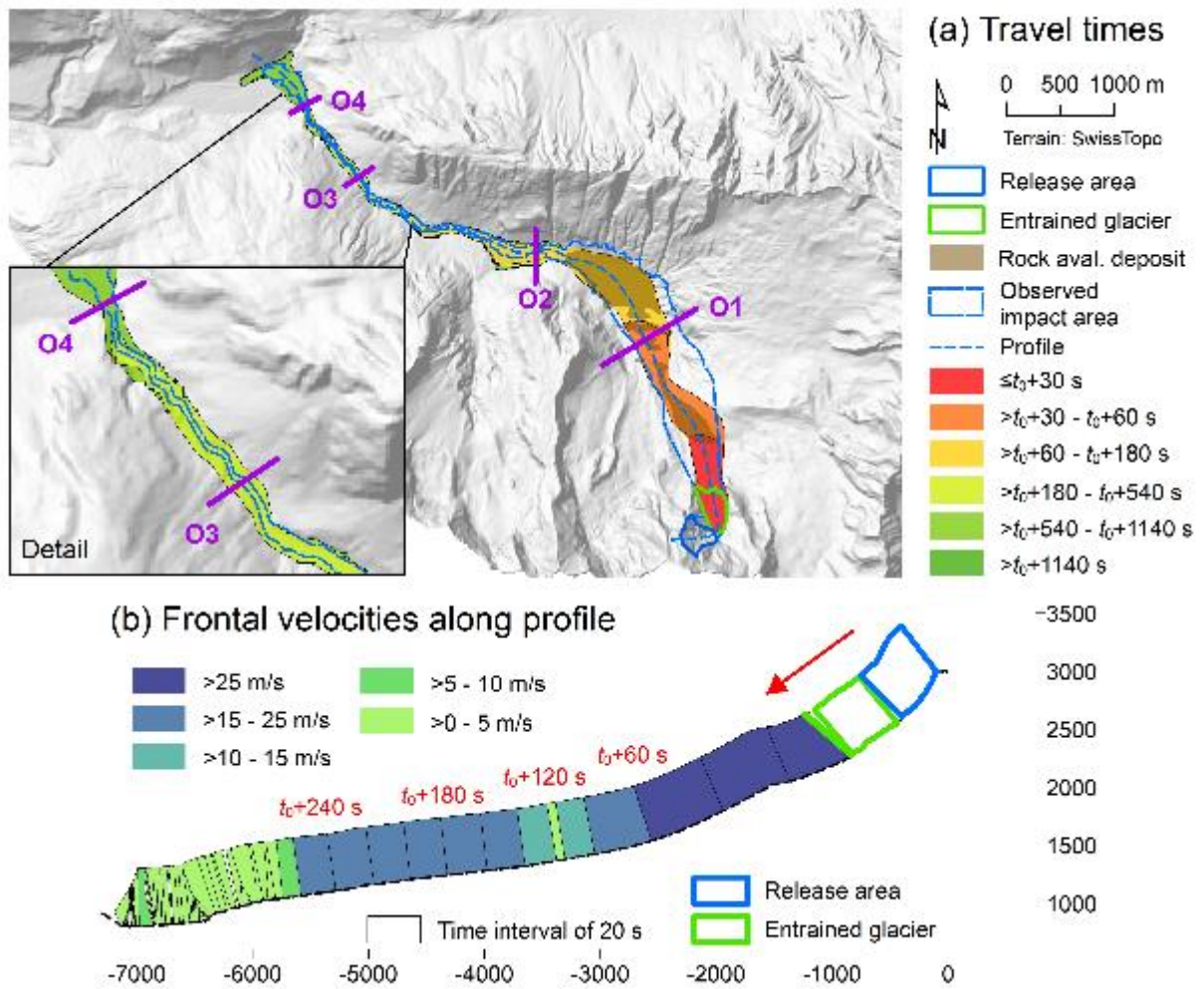
627
 628 **Figure 9.** Output hydrographs OH2 and OH4 derived for the scenarios S1 and S2. (a) OH2 for Scenario S1. (b) OH4 for
 629 Scenario S1. (c) OH2 for Scenario S2. (d) OH4 for Scenario S2. See Fig. 7 and Fig. 8 for the locations of the hydrograph
 630 profiles O2 and O4. H_s = solid flow height; H_f = fluid flow height; Q_s = solid discharge; Q_f = fluid discharge.
 631



632 **Figure 10.** Spatio-temporal evolution and velocities of the event obtained for **Scenario S1**. (a) Travel times, starting
 633 from the release of the initial rock slide-rock fall. (b) Frontal velocities along the flow path, shown in steps of 20 s.
 634 Note that the height of the velocity graph does not scale with flow height. White areas indicate that there is no clear
 635 flow path.
 636
 637



638
 639 **Figure 11.** Maximum flow height and entrainment derived for **Scenario S2**. RA = rock avalanche; the observed RA
 640 terminus was derived from WSL (2017).
 641



642 **Figure 12.** Spatio-temporal evolution and velocities of the event obtained for **Scenario S2**. (a) Travel times, starting
 643 from the release of the initial rock slide-rock fall. Thereby t_0 (s) is the time between the release of the rock slide-rock
 644 fall and the mobilization of the entrained glacier. (b) Frontal velocities along the flow path, shown in steps of 20 s.
 645 Note that the height of the velocity graph does not scale with flow height. White areas indicate that there is no clear
 646 flow path.
 647
 648